UNIVERSITY OF AMSTERDAM

UvA-DARE (Digital Academic Repository)

Spike-based coupling between single neurons and populations across rat sensory cortices, perirhinal cortex, and hippocampus

Dorman, R.; Bos, J.J.; Vinck, M.A.; Marchesi, P.; Fiorilli, J.; Lorteije, J.A.M.; Reiten, I.; Bjaalie, J.G.; Okun, M.; Pennartz, C.M.A.

Link to publication

OXFORD

Spike-based coupling between single neurons and populations across rat sensory cortices, perirhinal cortex, and hippocampus

Reinder Dorman[1,*], Jeroen J. Bos[1,2], Martin A. Vinck[1,3], Pietro Marchesi[1], Julien Fiorilli[1], Jeanette A.M. Lorteije[1], Ingrid Reiten[4],

Jan G. Bjaalie[4], Michael Okun[5], Cyriel M.A. Pennartz[1]

[1]Systems and Cognitive Neuroscience Group, SILS Center for Neuroscience, University of Amsterdam, 1098 XH Amsterdam, The Netherlands,
[2]Donders Institute for Brain, Cognition and Behavior, Radboud University, 6500 HC Nijmegen, The Netherlands,
[3]Ernst Strüngmann Institute for Neuroscience in Cooperation with Max Plank Society, 60528 Frankfurt, Germany,
[4]Institute of Basic Medical Sciences, University of Oslo, NO-0316 Oslo, Norway,
[5]Department of Psychology and Neuroscience Institute, University of Sheffield, Sheffield S10 2TN, UK
*Corresponding author: Systems and Cognitive Neuroscience group, SILS Center for Neuroscience, University of Amsterdam, 1098 XH Amsterdam,
The Netherlands. Email: r.dorman@uva.nl

Cortical computations require coordination of neuronal activity within and across multiple areas. We characterized spiking relationships within and between areas by quantifying coupling of single neurons to population firing patterns. Single-neuron population coupling (SNPC) was investigated using ensemble recordings from hippocampal CA1 region and somatosensory, visual, and perirhinal cortices. Within-area coupling was heterogeneous across structures, with area CA1 showing higher levels than neocortical regions. In contrast to known anatomical connectivity, between-area coupling showed strong firing coherence of sensory neocortices with CA1, but less with perirhinal cortex. Cells in sensory neocortices and CA1 showed positive correlations between within- and between-area coupling; these were weaker for perirhinal cortex. All four areas harbored broadcasting cells, connecting to multiple external areas, which was uncorrelated to within-area coupling strength. When examining correlations between SNPC and spatial coding, we found that, if such correlations were significant, they were negative. This result was consistent with an overall preservation of SNPC across different brain states, suggesting a strong dependence on intrinsic network connectivity. Overall, SNPC offers an important window on cell-to-population synchronization in multi-area networks. Instead of pointing to specific information-coding functions, our results indicate a primary function of SNPC in dynamically organizing communication in systems composed of multiple, interconnected areas.

Key words: brain state; multi-area networks; network dynamics; population coupling; spatial selectivity.

Introduction

Computations in the mammalian brain require coordinated activity of networks of interconnected neurons (DeCharms and Zador 2000; Harris et al. 2003; Barthó et al. 2004; Yuste 2015; Perich and Rajan 2020). For example, computations underlying the transformation of sensory information into episodic memory and subsequent memory retrieval are thought to require bidirectional communication between cortical sensory areas and (para)hippocampal areas (Buzsáki 1989; Squire and Zola-Morgan 1991; Eichenbaum 2000; Battaglia et al. 2011; Whittington et al. 2020). Such multi-area networks composed of local networks have been dubbed "meta-networks" to denote the requirement for a higher order of integration across the brain than can be achieved within single structures such as primary visual cortex (Pennartz 2015, 2022). These networks are subject to anatomical and physiological constraints, such as decreasing likelihood of having connectivity with increasing distance (Ercsey-Ravasz et al. 2013; Wang and Kennedy 2016). Although brain-wide networks have been investigated with anatomical methods (e.g. Harris et al. 2019), functional connectivity need not align with anatomy per se. A method to assess a theoretical framework for understanding meta-networks is to consider the functional relationships between spiking activity of single neurons and neuronal populations, quantified by cross-correlating single unit and population spiking activity (Okun et al. 2015). The strength of this single-neuron population coupling (SNPC) reflects the relationship between activity of the reference cell and the population's dynamics.

Here, we examined multi-area network dynamics by assessing SNPC within and between four distinct cortical areas in freely moving rats performing a figure-8 maze task, as well as during quiet wakefulness and non-REM (NREM) sleep. To study population coupling along the sensory-to-hippocampal hierarchy, we recorded cells from primary visual cortex (V1), the barrel field of primary somatosensory cortex (S1BF), hippocampal area CA1, and perirhinal cortex (PER). Although strong SNPC within a single cortical area has been reported (Bachatene et al. 2015; Okun et al. 2015, 2019), we predict this to be markedly less strong and less temporally precise between different brain structures, depending on anatomical and physiological constraints such as distance (cf. Wang and Kennedy 2016; Clancy et al. 2019). Furthermore, we expect functional and anatomical relationships between areas to be reflected in the SNPC. For instance, previous data indicate that primary sensory areas have modest levels of direct connectivity (Garner and Keller 2021; Iurilli et al. 2012; Meijer et al. 2017, 2019; Miller and Vogt, 1984; Oh et al. 2014; Van Strien et al. 2009;

Zakiewicz et al. 2014). Sensory inputs are known to reach the hippocampus indirectly via the perirhinal and postrhinal cortex (Burwell and Amaral 1998; Naber et al. 1999, 2000; Agster and Burwell 2009; Zakiewicz et al. 2014), but not directly—which predicts stronger coupling from sensory cortices to PER than to hippocampus. Lastly, in contrast to pyramidal cells, one may expect putative Fast Spiking (FS) interneurons to be coupled mainly locally.

The availability of both within- and between-area SNPC data also raises the question how these two forms of coupling are related (cf. Clancy et al. 2019). In other words, are there "hub" or "broadcasting" cells that do not only display local synchrony, but also regulate dynamics and information-processing in distant populations (cf. Stevens and Zador 1998)? An alternative configuration holds that individual neurons mediate only one type of coupling, so that some engage strongly only in local interactions, whereas others couple strongly to external, but not local populations. Multi-area SNPC analysis allowed us to investigate whether single cells are specifically coupled to only one target area or show a broadcasting configuration where each neuron couples to multiple areas, which may support a role of single neurons in meta-network functioning. We hypothesize that a higher degree of external broadcasting of a cell coincides with strong local synchrony.

SNPC may be governed by hard-wired connectivity and internal systems dynamics (Okun et al. 2015), but possibly also by behavioral factors, such as the subject's navigation through space and the correlative dynamics arising from hippocampal cells having nearby place fields (O'Keefe and Dostrovsky 1971). Thus, we investigated whether SNPC correlates with spatial coding by CA1 and neocortical cells. Furthermore, If SNPC values primarily depend on behavioral variables, one would not expect SNPC relationships to be conserved across different brain states. If, in contrast, SNPC is governed by hard-wired connectivity and intrinsic dynamics, we would expect SNPC and levels of broadcasting to remain similar across brain states.

In summary, we address four questions on SNPC within and across sensory cortical and (para)hippocampal areas: (i) How does SNPC within and between areas differ across various cortical areas, and does this follow known anatomical and functional constraints? (ii) Are levels of within and between-area population coupling correlated? (iii) Are there neurons that couple strongly to populations in multiple areas? (iv) Is SNPC mediated by fixed, intrinsic properties or is it governed by the dynamics associated with behavioral activity and concomitant spatial coding? The consequences of our findings for thinking about the structure and functioning of meta-networks will be addressed in the Discussion.

Materials and methods
Behavioral apparatus and task

All experiments were conducted in accordance with the National Guidelines on Animal Experiments and were approved by the Animal Experimentation Committee of the University of Amsterdam. Details of the experiment were previously described in Bos et al. (2017). Briefly, food restricted rats ($n = 3$) were trained to perform a two-choice visual discrimination task on a figure-eight maze (Fig. 1A, B, 114 cm × 110 cm). The animal was confined to the middle arm until a tone indicated a trial could be started by approaching the front barrier in the middle arm and breaking a photobeam, placed just before the front barrier. This triggered the onset of a visual stimulus on two monitors at the end of the middle arm with a 1-s delay. Visual stimuli were two equiluminant

wingding-font symbols; a plane and a diamond, defined as the conditioned stimuli CS+ and CS−, respectively. These were presented on two monitors placed in front of the initial arm segments of the maze; one of the monitors displayed a CS+ stimulus and the other one the CS− stimulus. Which monitor displayed the CS+ or CS− changed from trial to trial in a manner unpredictable to the rat. Visual stimuli were presented until the animal ventured in either the right or left arm and passed a "point of no return". Part of each arm was covered with sandpaper to provide tactile stimulation, and the coarseness of the texture was associated with the size of the reward in case of a correct trial. When the rat chose to enter the arm corresponding to the CS+ location, it received a food reward at the end of that arm. Choosing the arm marked by the CS− did not result in reward. Upon returning to the middle arm, an additional smaller food reward was delivered. Animal position was estimated with photobeams at several points on the maze, as well as with an overhead video-camera. The three animals (which were the same as used in Bos et al. 2017) were subjected to 12, 12, and 17 sessions, respectively, performing 60.1 ± 18.7 trials (mean ± SEM) per session. Sessions were on average $6{,}293 \pm 543$ s long. To assess sleep states, recordings were appended with a period of sleep after task performance (TP), which was done for two animals for 9 and 12 sessions, respectively. Total length of sleeping session were on average $1{,}774 \pm 390$ s (mean ± SEM). Additional details have been described in (Vinck et al. 2016; Bos et al. 2017).

Electrophysiological data acquisition

We performed simultaneous tetrode recordings in S1BF, V1, PER, and CA1. These areas are of interest because rats are highly skilled in using tactile abilities while exploring their environment; the visual modality had to be used to make correct choices in the task; the hippocampus is involved in spatial representations and memory, and PER is situated as a higher-level, multimodal cortical area with direct and indirect connections to the hippocampal region. After behavioral training, the animals were implanted with a custom-made microdrive ("quaddrive"; Technology Center, Faculty of Science, University of Amsterdam), consisting of 36 tetrodes, split equally over four areas: V1, S1BF, hippocampal area CA1, and PER (Fig. 1C, D). Tetrodes were gradually lowered for 8–10 days after implantation, and depth was estimated by the number of turns of guide screws (Lansink et al. 2007). Tetrode localization was later verified by anatomic reconstructions of tetrode tracts based on registration of histological section images to the Waxholm Space Atlas of the Sprague Dawley rat Brain v3 (Fig. 1D; RRID: SCR_017124; Papp et al. 2014; Bjerke et al. 2018), using the software tool QuickNII (RRID: SCR_016854; Puchades et al. 2019). Coordinates of the craniotomies relative to bregma were: V1 at −6.0 mm posterior, −3.2 mm lateral; S1BF at −3.1 mm posterior, −5.1 mm lateral; PER at −5 mm posterior, −5 mm lateral; CA1, −3.5 mm posterior, −2.4 mm lateral. Within each area, a separate reference electrode was inserted. Neural activity was recorded with a 128-channel Digital Neuralynx Cheetah Setup (Neuralynx, Bozeman MT). Spiking activity was extracted from bandpass filtered (600–6,000 Hz) signals, which digitized one millisecond epochs at 3 kHz when a pre-set voltage threshold was crossed. Single units were isolated by semi-automated spike sorting (KlustaKwik, Ken Harris, and MClust 3.5, A.D. Redish). A total of 1,781 neurons was recorded; the cell counts per animal were 456, 226, and 1,086 neurons. From S1BF, V1, PER, and CA1, we recorded on average 10.2, 2.4, 16.4, and 15.6 neurons per session, with a maximum of 32, 15, 40, and 72 neurons per session, respectively. Some sessions did not contain any neurons in a given
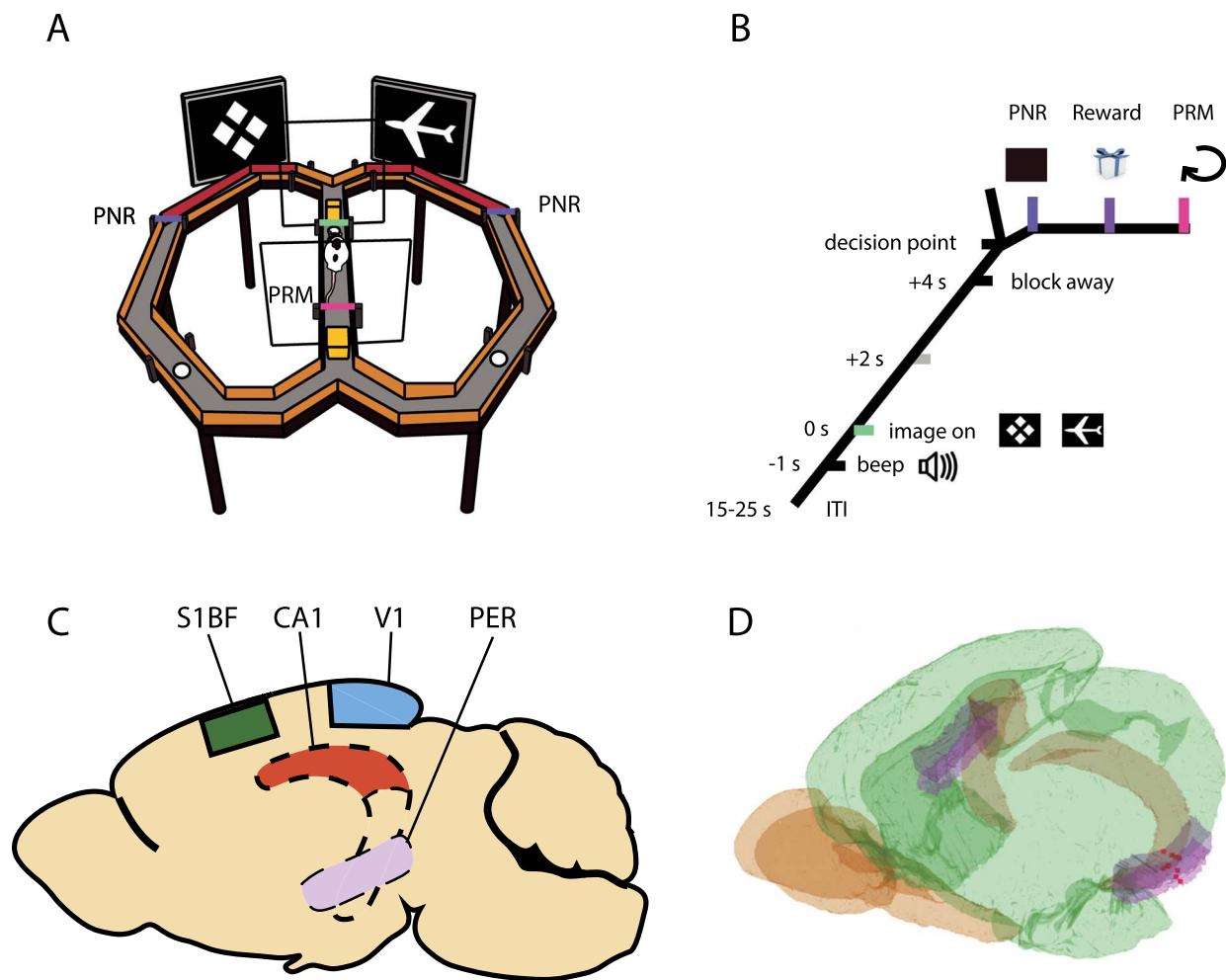
Fig. 1. Animals performed a behavioral task on a figure-8 maze, during which recordings were performed from S1BF, V1, PER, and CA1. (A) A schematic depiction of the figure-8 maze. Images were presented on monitors along the initial segments of the alleys. Crimson edges below the visual stimulus indicate sandpaper-walls. White dots represent reward wells. Green, blue, and magenta lines represent closable barriers in the animal's behavioral progression of the trial; a frontal barrier in the middle lane (green; trial start point), point of no return (PNR, blue) after which the animal cannot return to correct its decision, and the point of no return middle (PRM, magenta), the posterior barrier of the middle lane. (B) The temporal structure of the behavioral task. "Block away" marks the time point at which the green barrier was removed to enable the animal to execute its choice. ITI: intertrial interval. (C) Sagittal view of the recorded areas: S1BF (green), V1 (blue), PER (violet), and dorsal CA1 region of the hippocampus (orange). (D) Example 3D reconstruction of tetrode recording locations in PER of one animal. The red dots represent the reconstruction of the endpoints of respective tetrodes targeting the PER. A and B adapted from Bos., et al 2017.

area, and we used a threshold of minimum of 3 cells per session and area, otherwise said area was discarded from further analysis. Automated and manual clustering of spikes was performed based on waveform peak amplitude, energy, and first derivative of the energy. Clusters were accepted when the inter-spike interval of 2 ms was contaminated with $< 0.1\%$ of the total spike count. As interneurons can show narrow waveforms (Cardin et al. 2009; Gentet et al. 2010, 2012), we classified neurons as putative FS interneurons or putative pyramidal cells (cf. Vinck et al. 2016 for more details). For spatial linearization of the maze, it was segmented into 51 equally sized spatial bins (21 per each arm, 9 for the middle lane, bin length of ~ 9 cm). Rat position was assigned to a bin by assessing the minimal Euclidean distance between the rat's position and the bin centre position.

Analyses

Single-neuron population coupling. The goal of this analysis was to determine the temporal profile of population activity relative to the spikes fired by a single reference cell (Okun et al. 2015). The SNPC as calculated here is normalized for reference cell firing

rates and z-scored against a null-distribution (see below: *shuffling procedure*), allowing us to compare between cells and areas. Briefly, the SNPC quantifies how much a certain reference cell's activity is correlated with a certain population. Single-unit activity was collected in 1-ms bins. For each reference cell, the SNPC was calculated relative to the summed single unit activity of a target population, which could be recorded from the same brain area or a different one. When calculating within-area (i.e. internal or local) coupling, the reference cell was not included in the target population. Let the reference cell's firing rate be a $1 \times t$ vector R, with t being the duration of the recording period in ms. The target population firing rate was defined as the $N \times t$ matrix PR, where N is the number of single units in said target population. To compute the SNPC, the population rate PR was summed across all target neurons to yield the $1 \times t$ vector PR_{sum}. The SNPC was first calculated as the unscaled cross-correlation, specifically, the inner product of PR_{sum} with R at different lags (using MATLAB's *xcorr*), with a maximum positive and negative lag of 5,015 samples (5 s and 15 additional samples for edge-effect corrections). The outcome of this cross-correlation was normalized by the number

of spikes of reference cell R to correct for varying amounts of spikes per reference cell (i.e. by definition, more spikes would result in a higher outcome of this cross-correlation. The normalized cross-correlation was then convoluted with a Gaussian kernel (with a half-width of 12 ms, size of 15 samples). Edge effects due to the convolution were corrected by removing the outer 15 samples, resulting in a − 5 to +5 s SNPC.

Shuffling procedures. To determine the statistical significance of peaks or troughs in the SNPC cross-correlogram versus baseline activity and compare this appropriately between animals and sessions, we used a shuffling approach to generate a null distribution that served as a basis for Z-scoring. As sessions could differ in the number of neurons in the target population, we aimed to establish a null distribution based on the spiking activity of the reference cell and population in question, but in which coupling was abolished. While keeping the original reference-cell firing rate R, each row of the population rate matrix PR (i.e. firing rate of each neuron in the target population) was shuffled based on a circular temporal shift, with a maximal shift of plus or minus 50% of the entire recording length to get $PR_{shuffled}$. The circular temporal shift was shown to generate an appropriate null distribution (Fig. S1, comparing with a jitter shift shuffling of 100 ms). The $SNPC_{shuffled}$ was calculated from $PR_{shuffled}$ and R, as before. This shuffling procedure was repeated 1,000 times. The Z-scored SNPC cross-correlogram was acquired from the mean and standard deviation of all the $SNPC_{shuffled}$ versus the actual SNPC cross-correlogram. Physiologically meaningful coupling implies a significant deviation of the SNPC from $SNPC_{shuffled}$. The rationale behind this procedure is that, if the $SNPC_{shuffled}$ shows a high mean or variance, the actual SNPC needs to be corrected for such randomly generated cross-correlations. The level of coupling, expressed in standard deviations, was quantified as the peak value of the SNPC (where a peak is the highest value flanked by lower values, as determined by the MATLAB default peakfinding algorithm). We defined a cell as "coupled" if the SNPC was above a certain threshold std or higher above baseline, which also provided the basis for the Broadcasting Index (see also "statistical analysis," below). The threshold for coupling was based on a Bonferroni correction on the total amount of SNPCs calculated, i.e. the number of cells times the number of areas (i.e. 1,781 × 4), which was 4.5 std when rounded to one decimal. Negative coupling was quantified with the same algorithm, but looking for highest negative numbers.

Decoding of firing rate from population activity. Spike trains were first binned in 100-ms bins. The population rate was composed by summing the binned spike counts of all the cells in the population except for the seed cell. We then employed a K-fold cross-validation routine with five-folds to predict the binned spike counts of the seed cell from the population rate. We employed a linear regressor fit with stochastic gradient descent using ordinary least squares, as implemented in scikit-learn. Binned spike counts of both the seed cell and the population rate were standardized using mean and variance computed on the training set. To evaluate the performance of the regressor, we use the R^2 score (coefficient of determination), which takes a value of 1 when predictions are perfectly correct, and can be negative (models can be arbitrarily bad). An R^2 score of 0.2 indicates that the model can explain 20% of the variance in the data.

Spatial selectivity. Spatial selectivity was quantified in bits per spike (Skaggs et al. 1993):

$$I = \int_x \frac{r(x)}{r} \log_2 \frac{r(x)}{r} p(x) dx,$$

which calculates I, the spatial information (in bits per spike), where x denotes the current spatial bin, r(x) is the mean firing rate at bin x, r is the overall mean firing rate of the neuron, and p(x) is the probability density for the rat's position.

Clustering of CA1 spatial selectivity and coupling values was performed with a K-means clustering algorithm. Clustering was performed on log-transformed data, with the aim to find two clusters. For Fuzzy clustering, a Fuzzy C-means clustering algorithm (Fuzzy Clustering and Data Analysis toolbox, abonyilab. com/fclusttoolbox) was used. Here, cluster identity was defined by having a fuzzy partition above 0.75.

Non-REM sleep, quiet wakefulness and awake wakefulness. We compared three brain states: an awake but task-disengaged state during the inter-trial interval (ITI), TP, and NREM sleep. The ITI was identified as the period between the animal's return to the central arm (i.e. the start of the intertrial interval, ITI) and sound cue indicating onset of a new trial. This period lasted 19.0 ± 0.05 s (mean ± SEM) per trial. The TP period was taken from the active part of the trial and ranged from visual stimulus onset to the return to the central arm. This period lasted 23.5 ± 0.42 s (mean ± SEM) per trial. After the period of TP, the animal was allowed to sleep in a towel-covered flowerpot during which recordings continued. NREM sleep periods were identified by visual inspection of video footage and LFP traces as characterize by an absence of body movement and prominence of sharp wave-ripples and large-irregular activity (LIA) in the hippocampal leads (cf. Lansink et al. 2009). Bouts of NREM sleep lasted 47.7 ± 1.33 s (mean ± SEM) for a total of for 23 sessions.

Correlation coefficients between total coupling profiles of the different brain states were calculated for individual sessions. Individual sessions provided three *coupling profiles* (i.e. 4 × 4 matrices) for the three brain states, defined as the median coupling for each combination of available areas in said session. 2D correlations coefficients were calculated using MATLAB's *corr2*, for each session, between the three different brain states.

Statistical analysis. Under all conditions, and for all areas, levels of SNPC were not normally distributed, as shown by a Kolmogorov–Smirnov goodness-of-fit test. Hence, non-parametric testing was applied wherever possible. The Kruskal–Wallis test was used to determine an effect of each combination of reference and target area. The Wilcoxon's Rank-Sum test was used for pairwise comparison between different population coupling levels. Notably, the within- and between-area groups were handled separately because the marginally large SNPC values of the within-area group would skew any statistical analysis severely (note that the within-area group consisted of the four available areas coupled with themselves; between-area groups consisting of the four available areas coupled with the three other areas, resulting in a total of 12 combinations). Correlations were quantified using Spearman's rank correlation (within-area versus between-area coupling, spatial selectivity vs. coupling), or Pearson's correlation (Decoding accuracy). To identify significant effects of correlations, a Kruskal–Wallis test was performed on data binned along the explanatory variable (i.e. within-area in Fig. 4, spatial selectivity in Fig. 6). Bins were determined with the Freedman-Diaconis' method. The same statistical assumptions hold for the correlations between coupling levels and spatial selectivity. Lastly, if both brain area and brain state served as independent variables, we used a Schreier–Ray–Hare test, followed up by Wilcoxon's signed-rank (in paired conditions) or Wilcoxon's rank sum (in unpaired conditions) test for differences between states within one set of brain areas. All P-values of comparative and correlative statistics

were Bonferroni-corrected for the number of tests. Additionally, to verify key findings, we computed these on randomized halves of the data in a bootstrapping procedure (1,000 iterations); discrepancies have been indicated where applicable. Lastly, we define the Broadcasting Index (BI) as the number of areas a single cell is significantly coupled with (excluding the area containing that cell). To estimate how likely connections to two or three areas are, we compared bootstrapped (1,000 repetitions) significant connections (i.e. SNPC above 4.5 standard deviations, see *Methods: shuffling procedures*) to either two or three target areas with the joint probability calculated from probabilities of having any connecting to the respective target area. Here, we defined significance as having a joint probability outside of the 5 to 95% confidence intervals from the bootstrapped data (Fig. 5A, S12A). To compare percentages of cells with different broadcasting indices per area, a bootstrapping procedure (1,000 repetitions) was applied. Proportions of cells with a particular BI with nonoverlapping 5 and 95% confidence intervals were deemed significantly different (Fig. 5B, S12B).

Results
Within-area coupling

We performed tetrode recordings while rats ($n = 3$) navigated a figure-8 maze (Fig. 1A, B). We isolated single unit activity (total 1,781 neurons) from S1BF, V1, PER, and CA1 (Fig. 1C, D). For the SNPC, we calculated Z-scored, within-area coupling, cross-correlating single unit activity with summed population activity (Fig. 2A, S1). SNPC was calculated for all four areas, first assessed during active wakefulness. Our hypothesis held that within-area coupling would be homogeneous across the neocortical areas with likely stronger within-area coupling in the hippocampus, based on its strong propensity to generate synchronous rhythmic activity (Buzsáki 2010). Regardless of the brain area, over 80% of all cells showed a peak centered at zero lag (Fig. 2, Table 1), indicating that these cells were spiking often near-synchronously with numerous other units from the same population. In all areas, a number of cells showed a lack of a strong central peak, as expected from earlier studies in V1 (e.g. Fig. 2B; green lines in V1 plots and red line in PER plot; cf. Okun et al. 2015). A Kruskal–Wallis test indicated a strong difference between average levels of population coupling of the four areas (performed on only within-area data, Chi-square = 408.28, $P < 10^{-5}$, df = 3). Notably, we observed a higher level of within-area coupling in the hippocampus compared with perirhinal and sensory cortices (Fig. 2C; CA1 vs. S1BF, V1 and PER: all $P < 10^{-5}$, Wilcoxon's Rank-Sum test). In the somatosensory and visual cortex we observed similar levels of coupling. Lastly, perirhinal cortex showed significantly weaker within-area coupling compared with S1BF and area CA1 (both $P < 10^{-5}$, Wilcoxon's Rank-Sum test), but not visual cortex. In sum, these within-area coupling results are in line with earlier results on population coupling in V1 (Okun et al. 2015) and show a relatively large heterogeneity across the four areas, with area CA1 showing markedly high levels of within-area coupling. Negative within-area coupling, i.e. a trough around $t = 0$, was found in a smaller subset of cells distributed across areas (table 2). Negative coupling was generally smaller compared with positive coupling, and found not to be different between the four areas (Fig. S2).

High coupling rates would indicate that the local population rate can be informative of a certain reference cell's firing. Indeed, we found that a cell's population coupling strength correlates with the ability to decode the cell's activity from local population

activity (Fig. S3). Significantly coupled cells (i.e. with coupling value above 4.5 std, see Methods) show a significantly higher explained variance than non-coupled cells in perirhinal cortex and hippocampus, but this distinction was not significant in barrel cortex and visual cortex, due to higher variability of decoding accuracy in non-coupled cells.

Between-area coupling: general observations

Between-area coupling was studied by correlating activity of a single unit from one area with the population activity of another (Fig. 3A). We hypothesized that the coupling between two distinct sets of areas will conform to anatomical patterns of connectivity as described in the literature (see the specific sections below for references on the corresponding connections). Every single combination of areas contained single units displaying a noticeable peak around $t = 0$ (Fig. 3B, Table 1), signifying a cell being coupled between the two areas in question. Generally, between-area SNPC profiles were more temporally spread out, more variable and showed more complex shapes compared with within-area SNPC (i.e. in terms of peak-valley configurations, peak lags to zero, etc.; see Fig. 3B for examples). Detailed analysis of these complex shapes, performed e.g. by multi-Gaussian curve fitting or dimensionality reduction techniques, did not result in a systematic description of these highly variable profiles. Few neurons showed very high coupling, and on average, coupling values were lower than for within-area SNPC patterns (Fig. 3B, C, S4). These data indicate that a neuron's coupling to an external area is, on average, less tightly correlated in comparison to local coupling. A Kruskal–Wallis test indicated a strong difference in coupling levels for all between-area combinations (performed on only between-area data; Chi-square = 221.88, $P < 10^{-5}$, df = 11). For the sake of clarity, we will next discuss these between-area results in three categories: sensory cortices (S1BF and V1), perirhinal cortex, and hippocampus. The two sensory areas are deemed to have relatively similar neocortical circuitry, considerably different from perirhinal and hippocampus, as such they are grouped together (Douglas and Martin 2010; Harris and Shepherd 2015). Negative between-area coupling was also present, showing less differences between different area combinations (Fig. S5).

As was the case for within-area coupling, decoding a reference cell's spiking activity from population rates of other areas correlated significantly with its coupling values (Fig. S6), with the exception of reference S1BF cells relative to the V1 population and V1 cells to the PER population. Moreover, these two combinations showed no significant difference between mean decoder accuracies of coupled and uncoupled cells, whereas, for all other combinations, a clear and significant difference was found (Fig. S7). Thus, it generally appears that the activity of coupled cells can be decoded well from population activity in external areas, although this was not ubiquitously confirmed for all connections.

Coupling of sensory cortical neurons with populations in other areas

We expected to see coupling between sensory areas (Iurilli et al. 2012; Zakiewicz et al. 2014; Meijer et al. 2017), and from sensory areas to perirhinal (Burwell and Amaral 1998; Naber et al. 2000; Agster and Burwell 2009; Zakiewicz et al. 2014), as these areas have been shown to be directly anatomically connected. Moreover, sensory areas were not expected to couple strongly with the hippocampus due to their indirect connectivity (Naber et al. 2000; Zakiewicz et al. 2014). Assessing S1BF neurons in relation to V1 populations and vice versa we found a mean Z-scored coupling level of 4.83 (for $S1BF_{cell} - V1_{pop}$), and 6.42 std (for $V1_{cell} - S1BF_{pop}$),
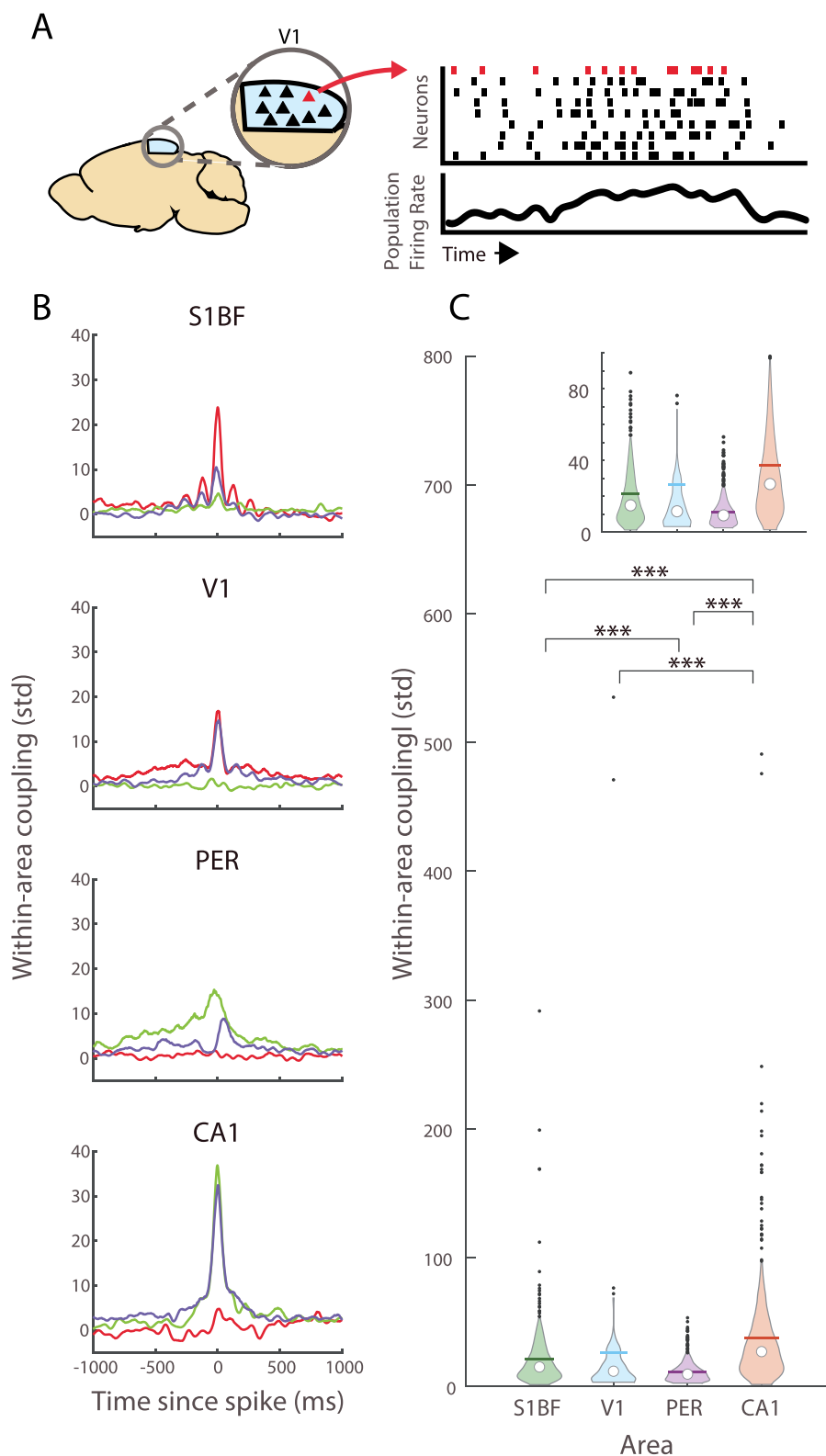
Fig. 2. Within-area single-neuron population coupling shows divergence between strongly and weakly coupled cells. (A) The within area SNPC was calculated from spiking activity within a single area (left, only V1 is depicted). V1 spiking activity is summed and cross-correlated with single unit activity (right), for example: comparing the red spikes with the total population activity (bottom right). (B) Representative SNPC within single areas, Z-scored to shuffled distribution, of three reference cells being coupled with the population within the same area, for each of the four recorded areas. Note the diversity in peak height, and the lack of a peak for some units, such as the green cell in V1. Each differently colored line indicates a different reference cell. Barrel cortex displays oscillatory activity in the low theta range (∼7 Hz) as noticeable oscillations in these graphs. (C) Violin plots showing spread and average of the within-area population coupling of all units of all animals. White dot: median; horizontal line: mean; black dots are > 95% percentile outliers. The areas are represented as green (S1BF), blue (V1), violet (PER), orange (CA1). Significance was assessed with Wilcoxon's Rank-Sum test: *** indicates $P < 0.0005$. P-values are Bonferroni corrected for six tests.
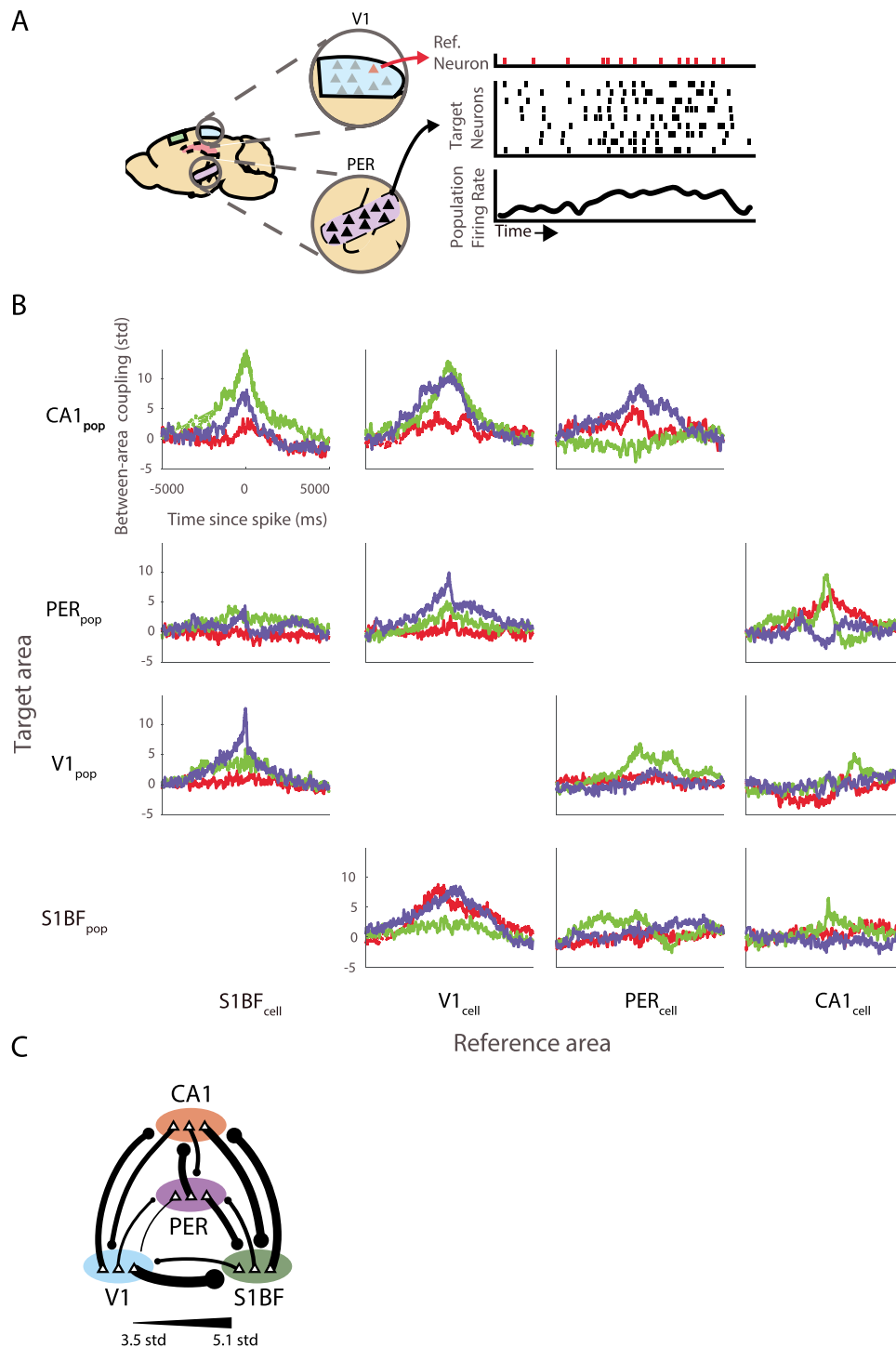
Fig. 3. Between-area SNPC shows how single neuron activity related across great anatomical distance to other populations. (A) Schematic illustration of between-area coupling, comparable with Fig. 2(A). The spike train of a single unit in a given area (e.g. V1, left) is correlated with the population activity of another area (e.g. PER). The red example neuron is cross-correlated with the total population rate of the target area (right). (B) Representative SNPC between areas, Z-scored to shuffled distribution, between different areas, excluding within-area coupling at the diagonal. Note a longer time range on the X-axis than used in Fig. 2(B). Columns correspond to reference areas, i.e. the areas to which the single neurons belong, rows correspond to the target areas, i.e. the areas to which the population rate signals belong. Differently colored lines per individual plot denote different cells from the reference area. Note the lower central peaks, and the broader temporal spread, compared with Fig. 2(B). As opposed to the within-area cases, most cells do not show strong coupling; however, several units are strongly coupled, e.g. the green line indicating an S1BF cell with the CA1 population. (C) Schematic depiction of median coupling levels across sessions, expressed as Z-scored SNPC, between the different cells and areas. Line thickness scales linearly with median coupling strength. Across all images the areas are represented as green (S1BF), blue (V1), violet (PER), orange (CA1). Triangles represent single units, the colored circles the entire population, i.e. a line from one triangle in V1 to the S1BF population depicts the median strength of V1 cells to the S1BF population.

and noticeable spread to higher values, with outliers above 20 std (Fig. S4). These outliers represent single neurons with very strong spike synchronization relative to the other sensory cortical area. Interestingly, V1 units were more strongly coupled to the S1BF population than the other way around (Fig. 3C, S4, $P < 10^{-5}$, see also table 3). Next, our data showed low coupling of sensory areas with perirhinal cortex compared with coupling of the two sensory areas to each other. Lastly and surprisingly, S1BF cells showed significantly elevated coupling with CA1 populations compared with other target areas ($P < 0.0005$, Wilcoxon's Rank-Sum test), whereas V1 cells lacked strong coupling with the CA1 population. However, the coupling of both sensory areas to CA1 showed noticeable outliers. $V1_{cell}$-$CA1_{pop}$ and $S1BF_{cell}$-$CA1_{pop}$ coupling did not differ significantly. For an overview of testing for statistical significance, see table 3. These results indicate that spike-based coupling between sensory areas and parahippocampal areas diverges from predictions based on anatomy.

Coupling of perirhinal neurons with populations in other areas

As an area intermediate between sensory areas and hippocampus, perirhinal cortex was expected to be coupled with both sensory areas (Burwell and Amaral 1998; Naber et al. 2000; Agster and Burwell 2009; Zakiewicz et al. 2014) and hippocampus (Burwell and Amaral 1998; Naber et al. 1999; Agster and Burwell 2009). Moreover, perirhinal neurons locking to CA1 theta oscillations (Bos et al. 2017) may be expected to show strong coupling. However, of all four areas studied, perirhinal neurons showed the lowest level of between-area coupling, with less outliers (Fig. 3, S4, table 1). PER cells engaged in significant SNPC with the sensory cortices, albeit less than SNPC levels between these two sensory areas. PER neurons coupled noticeably less with V1; in this respect their coupling was similar to that of V1 neurons, showing low coupling with PER populations. PER neurons showed stronger coupling to hippocampal populations ($PER_{cell} - CA1_{pop}$) and S1BF ($PER_{cell} - S1BF_{pop}$) than to V1 populations ($P < 10^{-5}$, Wilcoxon's Rank-Sum test, table 3), which was of a comparable level as the sensory neurons with CA1 populations (i.e. not significantly different). Interestingly, the overall coupling profile does not appear to differ much from the other two neocortical areas. These results highlight PER as an overall weakly coupled area, but its strong coupling with CA1 populations agrees with earlier anatomical and physiological studies.

Coupling of hippocampal neurons with populations in other areas

The hippocampus was expected to be well connected with the perirhinal cortex (Burwell and Amaral 1998; Naber et al. 1999; Agster and Burwell 2009), and to a lesser extent with sensory areas (Naber et al. 2000; Zakiewicz et al. 2014). Our data showed a modest level of functional coupling for $CA1_{cell} - PER_{pop}$ (Fig. 3, S4), comparable with the value of PER_{cell}—$CA1_{pop}$ coupling, and with relatively less strong coupled outliers (e.g. below 20 std, Fig. S4). Area CA1 cells showed similar levels of coupling with sensory cortices, noticeably with strong outliers, especially with the V1 population. CA1 cell couplings to all three target areas were not significantly different from each other (Fig. S4, table 3, $P > 0.05$, Wilcoxon's Rank-Sum test). Thus, unlike the anatomic connectivity would suggest, CA1 cells are similarly coupled to the sensory cortical areas and to PER populations.

Cell types

Fast spiking (FS) interneurons and pyramidal neurons were classified by way of waveform shape and firing characteristics (putative interneurons, $n = 188$; putative pyramidal neurons, $n = 1593$). We hypothesized FS interneurons and pyramidal neurons to show markedly different coupling profiles, with FS interneurons being strongly locally interconnected, whereas pyramidal neurons were expected to be more strongly coupled to more distant populations. However, when putative pyramidal and FS interneurons were analyzed separately, within-area coupling showed a similar pattern as when all neurons were combined, accompanied by roughly similar significant differences (albeit different *P*-values, Fig. S8). An exception was found for the two sensory areas: FS interneurons in S1BF showed higher within-area coupling than V1 FS interneurons, which was not the case for pyramidal cells. FS interneurons showed an overall higher level of within-area coupling than pyramidal cells, yet this was only significant for area CA1 (Wilcoxon Rank-Sum, pyramidal neurons vs. FS interneurons for CA1, $P < 10^{-5}$) and to a lesser extent S1BF ($P < 0.05$; see table 4 for statistical testing of differences between within-area coupling for pyramidal and FS interneurons).

As concerns between-area coupling, putative FS interneurons and pyramidal cells showed a surprisingly similar pattern (Fig. S9). Overall, FS interneurons tended to show higher levels of coupling to other areas than pyramidal cells, although this was only significantly different for three areas (table 5), most noticeably for $CA1_{cell} - S1BF_{pop}$. Thus, the overall pattern we observed when all cells were combined, as described above, was largely preserved for the two different neuron types (see table 5 for statistical testing of differences of all between-area coupling combinations for the two different cell types; see table 6 for statistical testing of between-area coupling of pyramidal cells versus FS interneurons).

Intra-areal coupling selectively correlates with inter-areal coupling

Could there be a relation between a cell's local and global coupling patterns? If single cells can play a pivotal role in regulating meta-network activity, one might expect a cell's within-area coupling to be predictive of between-area coupling: a strongly locally connected cell may be in an ideal situation to convey information to an external target. Fig. 4 displays the relations between within- and between-area coupling for four reference areas to selected target areas with linear regressions displayed for significant correlations (see Fig. S10 for individual plots for all reference-target combinations). Data showed mostly moderate to weak correlations between within-area coupling and between-area coupling. Interestingly, S1BF showed a significant correlation between its within-area coupling and its coupling to CA1. A similar trend was seen for visual cortex (i.e. V1 within-area versus $V1_{cell} - CA1_{pop}$, where the linear regression was relatively flat despite an increased spread with rising within-area coupling values (Fig. S10, second column, top row). Both sensory areas lacked a significant correlation between their within-area coupling and their coupling to the PER population. PER cells showed overall low Spearman's rho values between their within-area coupling and all target areas, indicative of a general lack of within-area SNPC correlation to connected areas. Lastly, within-area coupling of CA1 cells was significantly correlated with coupling to S1BF and PER populations, but not with V1. Overall, we find several connections showing positive correlations between external and internal coupling; however, this was not invariantly shown in all area-to-area combinations.

Broadcasting index

To quantify in more detail how cellular coupling to populations diverges—or broadcasts—across multiple areas, we defined a broadcasting index (BI). The BI is the number of target areas to
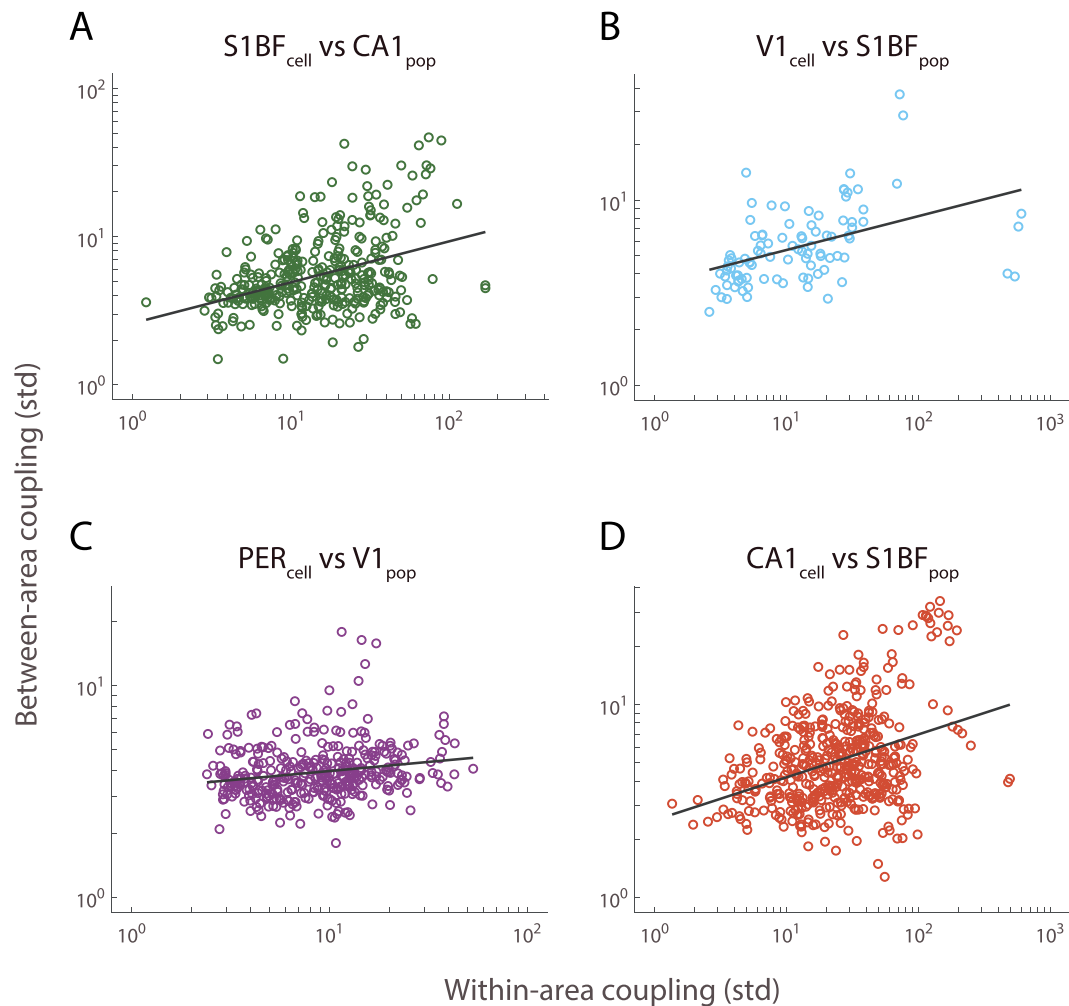
Fig. 4. Positive correlations between within- and between-area coupling. Scatterplots of within-area coupling versus between-area coupling strength for the four reference areas with one selected target area (A–D). *X*-axis indicates the within-area coupling strength of the reference area, *Y*-axis indicates the coupling of said reference area with the target area (indicated in the title as "Ref$_{cell}$ vs Target$_{pop}$"). Each dot represents one cell. Target areas were selected based on the significance of their correlations (a complete overview of all the areas is given in Supplementary Fig. S10). Black lines are linear regressions on log-transformed data. Correlations are quantified as Spearman's rho (from A to D: $\rho = 0.28$, $P < 10^{-5}$; $\rho = 0.57$, $P < 10^{-5}$; $\rho = 0.23$, $P = 0.00015$; $\rho = 0.28$, $P < 10^{-5}$). P-values were Bonferroni corrected for 12 tests. Across all images the reference areas are represented as green (S1BF), blue (V1), violet (PER), orange (CA1).

which the cell under scrutiny significantly couples (4.5 std above shuffled distribution; see Methods). By definition, for each cell this value ranges from 0 (no significant coupling) to 3 (significantly coupled to all three target areas). Within-area coupling was not included in the BI. We hypothesized that high-broadcasting cells (BI of two or three) are found in every area, with a higher number in CA1 and perirhinal cortex, because these areas are thought to be hierarchically well-positioned to broadcast to many neocortical areas (Squire et al. 1989; Fiorilli et al. 2021). Much like the within-area versus between-area correlations described above, we would expect high-broadcasting cells to be strongly connected with their local population.

In every reference area, we found cells that broadcast to all three other areas (i.e. BI = 3), albeit that these constituted only a small minority of the total number of neurons (Fig. 5A). In all areas, we found that the number of cells with a BI of 3 exceeded what would be expected from the joint probability of the single connections, whereas a BI of 2 often appeared in lower numbers than expected (Fig. 5A). Furthermore, we observed a trend with V1 showing more broadcasting cells, yet an effect of area on the number of cells with a specific BI was not significant. Comparing

percentages of cells with a certain BI across all areas (Fig. 5), we saw a general reduction of the ratio of cells with higher broadcasting indices, yet between broadcasting indices 1 and 2 this diverged for the different areas: CA1 and V1 showed no significant difference between indices 1 and 2, while S1BF and PER showed a significant reduction in the number of cells with index 2 compared with 1 (based on bootstrap-estimated confidence intervals, see Methods). No significant differences between the four areas were observed for maximum broadcasting (BI of 3). Lastly, we expected a higher BI to be related to stronger local coupling. Interestingly, however, cells with different broadcasting indices did not show significantly different levels of within-area coupling, for all areas (Fig. S11).

Between pyramidal cells and FS interneurons (Fig. S12), we observed a similar overall decrease in the number of cells with higher broadcasting indices. FS interneurons showed a significantly higher percentage of cells with non-zero broadcasting indices in S1BF and CA1 (*P* < 0.05, bootstrap test), and showed an overall larger variation for each area (note that the total number of FS interneurons was roughly 7 times less than the number of pyramidal neurons, influencing statistical power and variability).
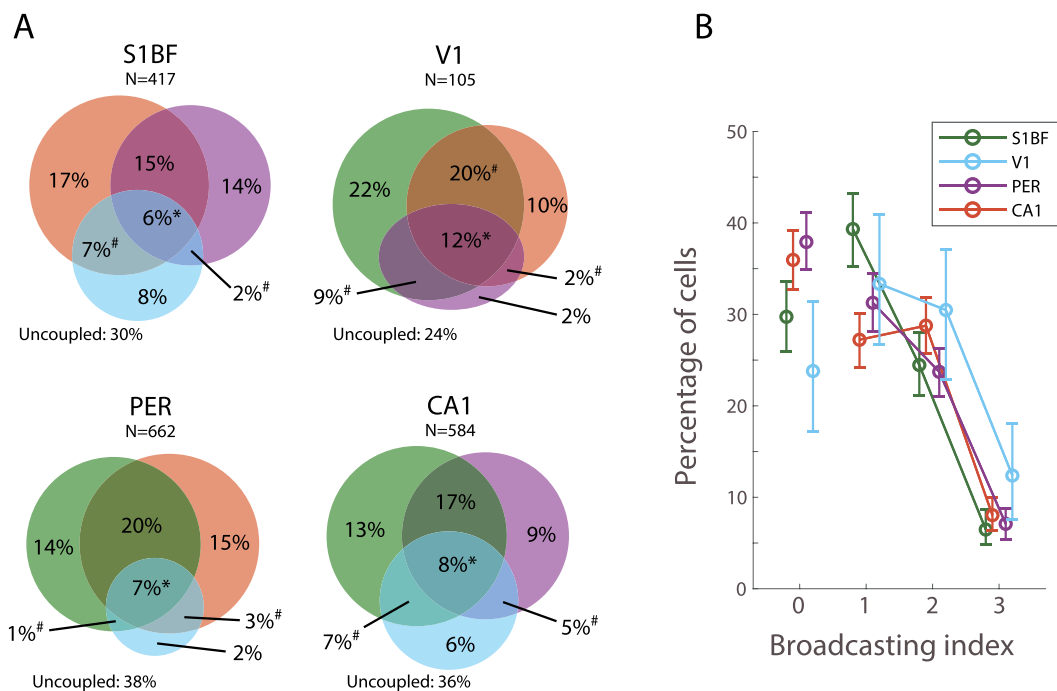
Fig. 5. Cells in sensory and (Para)hippocampal areas mostly show varying degrees of broadcasting. (A) Venn diagrams illustrating the percentages of cells having a significant number of coupling to the three available target areas. Asterisks and pound symbols show results for bootstrap testing ($\alpha = 0.05$) if connections to two or more areas are expected compared with the joint probability of cells connecting to one area. Asterisks indicate more cells than expected, and pound symbol less than expected. (B) Percentages of cells plotted as a function of broadcasting index. Confidence intervals are bootstrap estimates (1,000 iterations). Across all images the areas are represented as green (S1BF), blue (V1), violet (PER), orange (CA1).

FS interneurons in PER lacked coupling with V1, resulting in a lack of cells with a BI of 3. Similarly, pyramidal neurons as well as FS interneurons showed no effect of BI on within-area coupling (Fig. S13).

Summarizing, highly broadcasting cells were found in all areas, and we did not find strong differences between the examined brain areas. Broadcasting appears to be independent of the cell's coupling with its local population.

Population-coupled neurons and spatial selectivity

Within-area population coupling may reflect intrinsic neuronal parameters, largely invariant to cognitive computations. The contrasting hypothesis holds that SNPC does cohere with representational content coded in the area under scrutiny, such as spatial information coded in area CA1 (O'Keefe and Dostrovsky 1971). Regarding between-area coupling, we hypothesized that the spatial selectivity of CA1 cells may be correlated with strong coupling to sensory areas: if the spatial selectivity of CA1 cells is dependent on sensory inputs (Hartley et al. 2000; Jeffery 2007; Mehta 2015), coupling of spatially selective cells may be stronger with sensory areas as compared with non-selective cells. Spatial selectivity was calculated in bits per spike (Fig. 6A). As expected, we found high levels of spatial selectivity in a subset of CA1 cells during maze running (Fig. 6A, B). As reported before, a subset of PER neurons fired selectively for large maze segments (Bos et al. 2017) and a limited location-dependence was observed for both sensory areas (Lansink et al. 2018; Mertens et al. 2023), resulting in a low number of cells with high spatial selectivity (Fig. 6B). It should be noted that the apparent spatial selectivity of some S1BF and V1 cells may be partly explained by location-specific behaviors that impose local, sensory-specific changes (Mertens et al. 2023).

We found that, if correlations between spatial selectivity and population coupling were significantly different from zero, they

were negative (Fig. 6C). This negative correlation was significant for PER, CA1 and S1BF ($P < 10^{-5}$, $P < 10^{-5}$, and $P = 0.0076$, respectively, Wilcoxon's Rank-Sum test, $P < 0.05$ in an additional bootstrap test, see Methods) but not for V1 ($P = 1.2$, Wilcoxon's Rank-Sum test). As the SNPC is corrected for number of spikes and spatial selectivity is expressed in bits/spike, this effect cannot arise from lower numbers of spikes in cells with higher spatial information. Furthermore, CA1 showed two distinguishable clusters of higher and lower spatial selectivity (defined with K-means clustering, Fig. 6C and S14). When comparing SNPC in these separate clusters, we found a strong significant difference in within-area coupling between the low and high spatially selective groups (Fig. S14B, Wilcoxon's Rank-Sum test, $P < 10^{-5}$). Because some datapoints do not appear to clearly fall in a cluster, we applied fuzzy clustering and tested for differences between datapoints with a partition over 0.75 (Fig. S14C), which provided a comparable level of significance. Negative coupling was not significantly correlated with spatial selectivity, except weakly within S1BF (rho = −0.14, data not shown).

Next, we analyzed spatial selectivity versus between-area coupling. We found significant correlations between $CA1_{cell}$ and $S1BF_{pop}$, and reciprocally between CA1 and PER all with relatively low correlation coefficients (Fig. S15). Here, too, we were able to separate CA1 neuron couplings to different areas based on clear clusters of higher and lower spatial selectivity (Fig. S16). Differences in between-area coupling for the high and low spatially selective groups were only significant for the coupling of CA1 cells with PER populations (Fig. S16C, Wilcoxon's Rank-Sum test, $P < 10^{-5}$).

Dependence of coupling on brain state

To gain further insight into the dependence of SNPC on intrinsic state parameters vis à vis behavioral conditions, we asked whether coupling, analyzed so far in active wakefulness, is
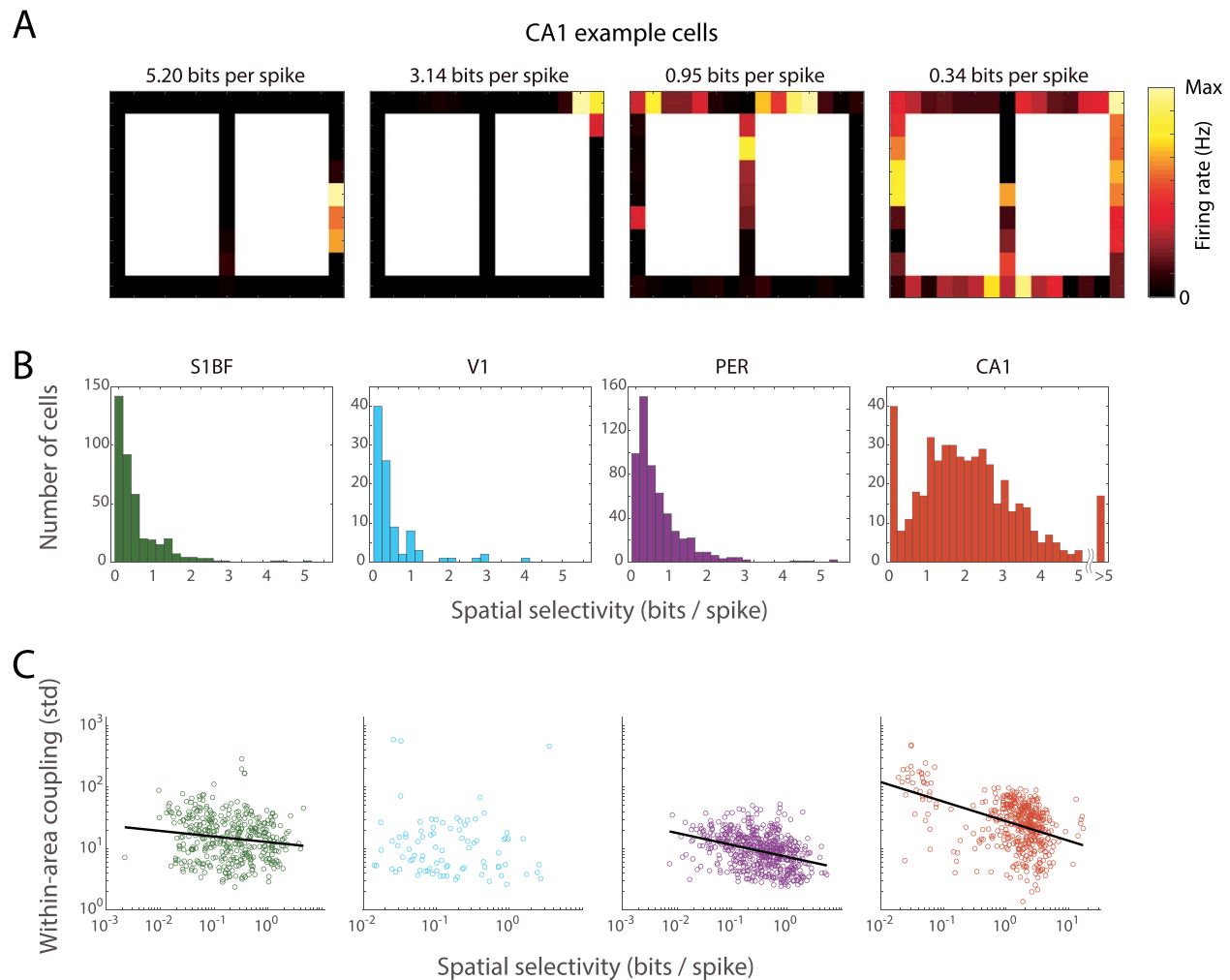
A

CA1 example cells

5.20 bits per spike   3.14 bits per spike   0.95 bits per spike   0.34 bits per spike

B

C

Fig. 6. Different areas display differing levels of spatial selectivity, correlated with within-area coupling in S1BF and CA1. (A) Examples of four CA1 cells' spatial responses on the figure eight maze and their respective spatial information in bits per spike. (B) Distribution of spatial selectivity in all four areas. (C) Spatial selectivity correlated with within-area coupling. Black lines are linear regressions on log-transformed data, only shown for significant correlations (from left to right: $\rho = -0.16$, $P = 0.0076$; $\rho = -0.11$, $P = 1.2$; $\rho = -0.38$, $P < 10^{-5}$; $\rho = -0.38$, $p = < 10^{-5}$). Note that the CA1 population appears to consist of two clusters of cells, based on their spatial selectivity. Across all images the areas are represented as green (S1BF), blue (V1), violet (PER), orange (CA1). All correlations are quantified as Spearman's rho. *P*-values in C are Bonferroni corrected for four tests.

affected by the brain state. We hypothesized that overall between-area coupling will decrease during NREM sleep, corresponding to decreased inter-areal communication as compared with active TP. In addition, we hypothesized that within-area coupling during sleep will increase relative to awake conditions. Lastly, we expected lower levels of between-area coupling in behaviorally active states (Olcese et al. 2016). We classified NREM sleep periods (NREM), ITI periods, and active TP. As expected, these different brain states show differential spiking activity, with NREM showing significantly decreased firing rates relative to ITI and TP (Fig. S17). First, we assessed brain state-driven differences between overall coupling profiles, i.e. the total profile of coupling of all areas with each other, as a 4×4 matrix. By calculating correlations between coupling profiles during the different brain states we observed that the total profile of coupling per session was different in NREM conditions versus ITI and TP (Fig. 7). ITI and TP were highly correlated, indicating no dramatic changes of the total coupling profile between these awake states. The lowest correlations were seen between NREM and TP, however, with a median still above 0.6, indicating that even amongst strongly different brain states, global coupling patterns remain comparable.

The levels of within-area population coupling were selectively affected by state, area and their interaction (Fig. 8A, Kruskal–Wallis, $P < 0.05$ for all four areas separately), but remained globally intact across all three states. Post hoc Wilcoxon's Sign-Rank tests indicated several significant differences per area. For the sensory areas, coupling in NREM was slightly but significantly elevated in S1BF. V1 displayed a reduced level of coupling in TP versus ITI, a result not shared with S1BF. Next, PER showed higher coupling during NREM versus the other two states. CA1 showed differences between all three states: the highest coupling was found in ITI, followed by TP and lastly NREM. Thus, although brain state has an effect on coupling levels, our hypothesis on a generalized increased within-area coupling in NREM sleep was not confirmed. Interestingly, CA1 did show a different pattern, displaying lower coupling in NREM.

For between-area coupling, we observed no unitary effect of state in all areas, such as a global loss during NREM sleep in between-area coupling (Fig. 8B, S18). In a first analysis, we found a statistical effect of state on coupling levels (Kruskal–Wallis, Chi-square = 106.66, $P < 10^{-5}$, df = 2). Specifically, we observed a decrease of coupling of CA1 to all three target areas during NREM,
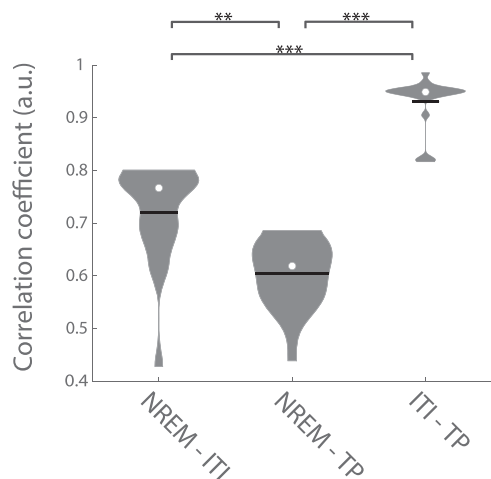
Fig. 7. Correlations of all coupling levels between different brain states, for each session. For each session, correlation coefficients of entire coupling profiles (i.e. all four areas with each other) for two brain states were calculated. The awake states (ITI and TP) are very strongly correlated, whereas NREM is significantly correlated (although less) with both awake states. White dot: median; horizontal line: mean. NREM: non-REM sleep, TP: task performing, ITI: inter-trial interval. Significance was assessed with Wilcoxon's sign-sum test: $**P < 0.005$, $***P < 0.0005$. P-values are Bonferroni corrected for three tests.

which was significantly lower than ITI and TP states (Wilcoxon's Sign-Rank, $P < 0.05$). Furthermore, PER_{cell} ➔ $S1BF_{pop}$ showed an increase in coupling in NREM sleep relative to ITI (Wilcoxon's Sign-Rank, $P < 0.0005$). However, a secondary analysis using a bootstrap procedure (1,000 iterations, with half the data per iteration used for cross-validation, comparing median distributions) failed to confirm these differences. Thus, although there appears to be a trend in levels of coupling from CA1 to other areas, no definitive conclusions can be drawn here on brain-state effects on inter-areal coupling.

Discussion

We investigated how single-neuron spike patterns correlate with population firing activity within and between sensory cortical and (para)hippocampal areas, with special emphasis on cross-areal interactions. Our main findings can be summarized as follows: (i) coupling of single neurons to their local population was prominent across all four areas investigated, and area CA1 showed a markedly stronger within-area coupling than the other areas (Fig. 2); (ii) between-area coupling showed broader and more variable temporal profiles than within-area coupling (Fig. 3); (iii) a majority of pairwise area combinations showed significant positive correlations of within- and between-area coupling, especially when involving area CA1 (Fig. 4, S10); (iv) broadcasting cells were found in all four areas, where higher broadcasting appeared uncorrelated with local coupling (Fig. 5); (v) negative correlations were found between spatial selectivity and within-area coupling in S1BF, PER, and CA1 (Fig. 6), and (vi) although within-area coupling patterns were subject to modulation by the brain state, we found no generalized strong effect of brain state on between-area coupling values (Fig. 8b). These results characterize the S1BF-V1-PER-CA1 system as a coherent, dynamic meta-network with heterogeneous degrees of internal and external coupling. In this multi-area system, coupling strengths appear not to be governed primarily by selective information processing expressed during behavior (e.g. spatial selectivity), but cohere

more strongly with intrinsic dynamic properties subject to non-homogenous modulation by the brain state across cortical areas.

Within-area coupling: contrast between hippocampus and perirhinal cortex

Our results on within-area coupling in rat cortex are largely in line with previous reports on mouse V1 (Okun et al. 2015) and prefrontal cortex (Okun et al. 2019). The two sensory cortical areas we investigated, S1BF and V1, showed comparable levels of within-area coupling, which is consistent with the general similarity in sensory neocortical wiring conforming to principles of canonical cortical microcircuits (Douglas and Martin 2004). CA1 harbors densely packed, synchronized populations, acting as a powerful dipole layer that generates high-amplitude LFPs to which neuronal firing locks (Buzsáki 2002; Csicsvari et al. 2003; Buzsáki 2010; Somogyi 2010; Yang et al. 2014). This rhythmic firing could be an important factor in accounting for the strong within-area coupling of CA1 neurons. Furthermore, the increased within-area coupling of FS interneurons in CA1 might link to their prominent role in regulating brain dynamics. Of the four areas studied, perirhinal cortex showed the lowest level of within-area coupling, albeit not significantly lower than V1. Although perirhinal cortex is usually deemed to conform to canonical cortical circuitry, it deviates in some aspects, such as a lower density of pyramidal neurons (Kealy and Commins 2011). PER has been described as an "inhibitory wall," gating information flow from the neocortex to hippocampus (Martina et al. 2001; de Curtis and Paré 2004; Pelletier et al. 2004) and PER has been reported to lack strongly synchronized activity (Pelletier et al. 2004). This might be reflected in the relatively low levels of within-area coupling of PER neurons.

Between-area coupling: deviations from predictions based on neuroanatomy

In general, between-area coupling was less strong than within-area coupling. Secondly, between-area coupling showed a broader temporal alignment with firing of the reference cell, spanning up to seconds compared with the sub-second range in within-area conditions. This difference was expected because connection probabilities decrease over longer anatomical distances (Ercsey-Ravasz et al. 2013), the involvement of poly- instead of monosynaptic circuitry likely increases with distance, and a given neuron in a remote target area likely receives inputs from many other afferent areas than from the area containing the reference cell alone. The underlying microcircuitry is not elucidated here and may involve "third sources" that provide common input driving activity of both the reference cell and target population. Indeed, population activities are likely not fully independent, due to the strong interconnectedness of cortical areas. Yet, the involvement of a third source does not negate this correlated activity as being functionally relevant.

We found asymmetric coupling levels between the two sensory cortical areas: V1 neurons showed significantly higher levels of coupling with S1BF populations than from S1BF neurons to V1 populations. (Fig. 3, S4, table 3). In line with this, a previous study reported phase-locking of V1 neurons to LFPs recorded from somatosensory cortex (Sieben et al. 2013). Theoretically, if firing rates in both sensory areas were the same, it would be statistically unlikely to have different coupling levels between two reciprocal connections (note that firing rates did differ between areas, e.g. Fig. S17, yet it is unknown how different firing rates affect coupling specifically). As yet, we can only speculate why the V1-S1BF coupling shows an asymmetry. During TP, intense whisker and other tactile inputs may predominate over visual
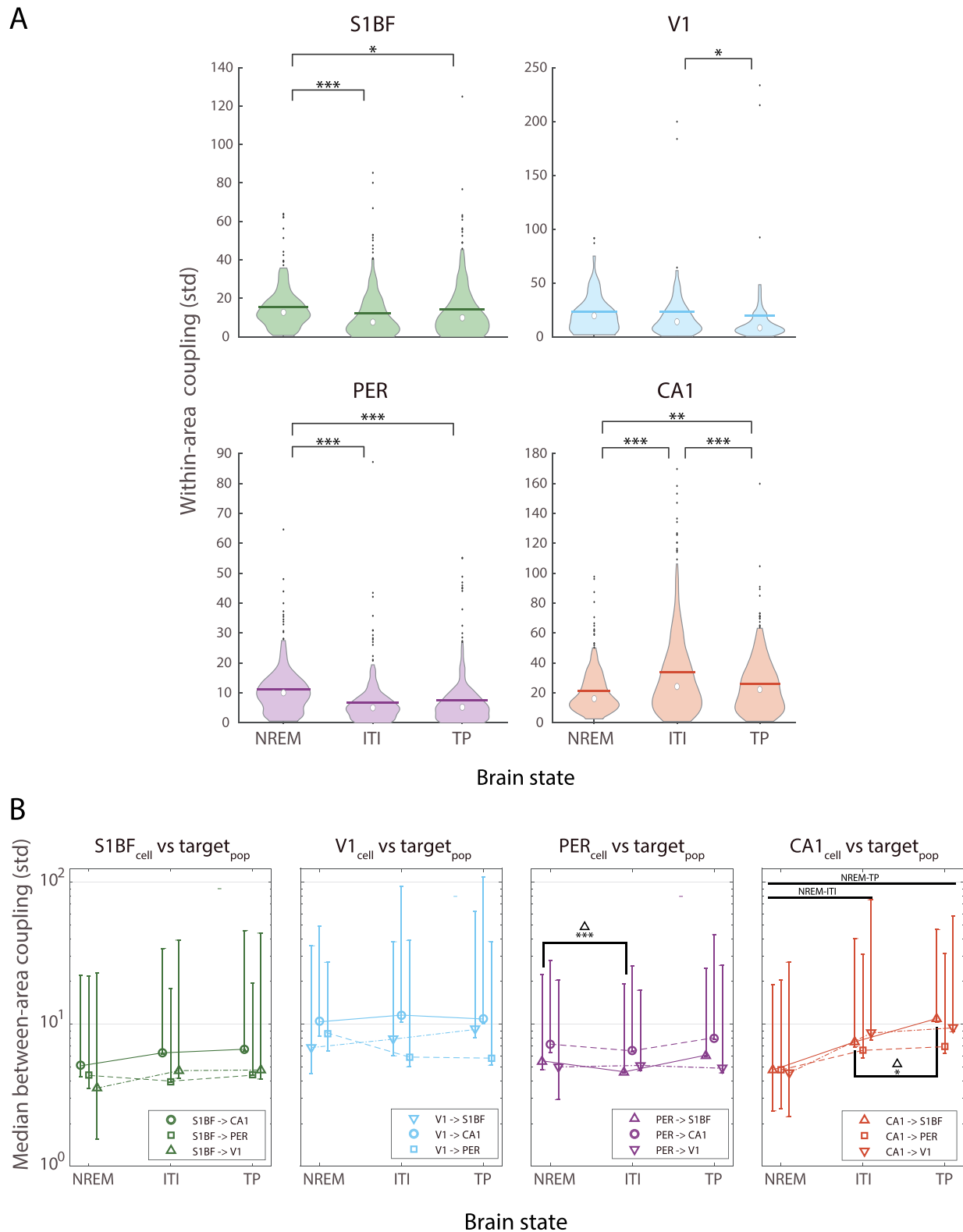
Fig. 8. Modulation of within- and between-area coupling by the brain state. (A) Violin plots of within-area coupling in the four areas in the three brain states. White dot: median; horizontal line: mean; black dots are > 95% percentile outliers. (B) Median of between-area coupling as a function of brain state. Error bars indicate 5–95% confidence intervals. Significance bars with symbols (e.g. the triangle) indicate which individual coupling value shows significant differences between brain states. Horizontal black bars in the rightmost plot indicate significance between brain states for all three target areas in question. Across all graphs, the areas are represented as green (S1BF), blue (V1), violet (PER), orange (CA1). NREM: non-REM sleep, TP: task performing, ITI: inter-trial interval. The significance of differences between coupling values in different brain states was assessed with Wilcoxon's Sign-Rank test: *$P < 0.05$, **$P < 0.005$, ***$P < 0.0005$; horizontal black bar in (B) indicates $P < 0.05$ for all three target areas in question. *P*-values are Bonferroni corrected for the number of tests (12 in A, 48 in B).

inputs, possibly resulting in stronger S1BF population synchrony than in V1. As yet, however, it is too early to ascribe this difference in coupling to sensory inputs arising during active behavior.

Strikingly, sensory cortical neurons showed higher coupling with CA1 populations than with the anatomically more proximal and more connected perirhinal cortex. Anatomic consensus holds that sensory cortical information is relayed via the perirhinal and postrhinal cortices to the hippocampus (Deacon et al. 1983; Burwell and Amaral 1998; Naber et al. 1999, 2000; Witter et al. 2000; Agster and Burwell 2009; Arszovszki et al. 2014; Zakiewicz et al. 2014). A strong between-area SNPC may, however, not only reflect sensory input to the hippocampus, but could also express how CA1 population output correlates with single-cell activity in sensory cortices. Such correlation might be driven by brain-wide effectors such as sensorimotor feedback. Likewise, the low coupling between sensory areas and perirhinal cortex diverges from the anatomically based prediction. Again, following the concept of PER as an "inhibitory wall," a sensory-to-hippocampal gating function may result in a sparsification of PER firing patterns, and hence may result in lower levels of coupling between PER and the sensory cortices. However, if PER would simply function to critically suppress neocortical inputs *en route* to the hippocampus, one would not expect the strong sensory-CA1 coupling like we observed (Fig. 3, S4). This strong coupling may be most parsimoniously explained by sensory cortical-hippocampal connections bypassing the PER (Naber et al. 1999; Agster and Burwell 2009; Goode et al. 2020; Fiorilli et al. 2021). In general, we note that fiber tracer studies can only provide a crude guidance in predicting SNPC relationships; they establish global innervation patterns but neither probe synaptic connectivity to specific cell types, nor synaptic strength. Thus, tract-tracing and spike-based studies reveal different aspects of interconnected networks and are largely complementary to each other.

Turning to the involvement of putative pyramidal cells and FS interneurons in within- and between-area coupling, we found surprisingly few differences. Although FS interneurons generally have only local, short-range connections, several studies on hippocampal and rhinal regions showed FS interneurons to project outside their area of origin (Apergis-Schoute et al. 2007; Jinno et al. 2007; Melzer et al. 2012). A possible explanation for the elevated between-area coupling of FS interneurons (Fig. S9) may be their role in synchronizing pyramidal neurons, which thereby involve these FS interneurons in between-area interactions via a polysynaptic route. In CA1 and S1BF, interneuronal within-area coupling was, on average, higher than for pyramidal neurons—a result that may likewise be explained by the entraining (i.e. temporal alignment) or synchronizing effect of interneuron activity on mass pyramidal cell activity within the same region (Csicsvari et al. 1999).

Within-area versus between-area coupling

For 9 out of 12 area-to-area combinations, we report significant positive correlations for within-area versus between-area coupling (Fig. 4, S10). This finding indicates that a locally coupled cell tends to couple significantly to an external population (Clancy et al. 2019), but it should be noted that most of the correlations had modest Spearman's rho values, implying a great degree of cell-to-cell variability in the relationship between internal and external coupling. Strong local synchrony, corresponding to within-area correlation, would indeed be expected to either correlate with strong afferent input to the same area, or be conducive to driving coordinated output—in both cases, leading to a stronger level of between-area coupling

(Stevens and Zador 1998; Zandvakili and Kohn 2016). Perirhinal cortex was the only target population where coupling with sensory neurons showed no significant correlation between within- and between-area coupling. Thus, positively correlated within- and between-area coupling does not represent a general connectivity rule. Interestingly, although strength of within- and between-area coupling correlate, the number of targets significantly coupled with, i.e. the broadcasting index, did not effect within-area coupling strengths (Fig. 5).

The "inhibitory wall" property attributed to the perirhinal cortex might act to transform cortical to parahippocampal activity, where neocortical input has a low probability of driving PER neurons to spiking (de Curtis and Paré 2004; Pelletier et al. 2004). This sparsification would indicate that sensory information gated in perirhinal cortex need not be from "hub"-like sensory neurons with strong local involvement, but from a broad range of sensory cells. Furthermore, the neocortical-to-parahippocampal transformative properties would predict that CA1 neurons also lack within-vs-between correlation with the sensory areas. However, CA1 neurons coupling with S1BF and V1 showed overall positive correlations. Although this might be explained by differential pathways of information transfer from neocortex to hippocampus (Somogyi 2010), the exact neuronal variables driving the differences in between-area coupling remain unknown.

Negative correlation between spatial selectivity and SNPC

The negative correlation we found between spatial selectivity and local population coupling of CA1 neurons was mirrored by similar findings in S1BF and PER (Fig. 6). At first sight, this negative relationship may seem surprising, but a strong functional connectivity of a given neuron to its local population may well be accompanied by a plethora of mixed inputs to this neuron, preventing it from generating a highly specific spatial code. Indeed, a recent study found synaptic glutamatergic input to non-place cells to be slightly but significantly higher than place cells (Adoff et al. 2021). Secondly, our findings indicate that high within-area SNPC is not driven by local neurons with high spatial selectivity. Had within-area coupling been driven by the animal's locomotor behavior leading to sequential activation of place cells in CA1, then a positive correlation would have been expected. Thus, SNPC in areas CA1 and S1BF is not strongly determined by cognitive computations underlying place tuning.

Modulation of population coupling by brain state

We report several differences in SNPC between awake (i.e. task-performing and non-performing states) and NREM sleep. First, the high correlation between the active and resting (ITI) awake states indicates that overt behavior has little effect on general patterns of coupling between brain areas, despite the need for sensory processing, goal-directed behavior, and reward expectation and consumption in the active state. The paradigm task at hand is unsuitable to investigate sensory processing and coupling in more detail. Furthermore, although within-area coupling patterns differed between the NREM condition and awake states, the correlation between these states was far from abolished, with average correlations in the range of 0.6 to 0.7. Thus, when comparing different brain states, coupling remains to a large extent driven by internal dynamics and not by sensorimotor inputs. During NREM sleep, we expected a general decrease in between-area coupling, but an increase in within-area coupling (Olcese et al. 2016). Within-area coupling indeed increased during sleep in most

areas, with CA1 being an exception. Furthermore, we did not find a clear decrease of between-area coupling between areas.

Although it is known that brain states affect the firing rate (Vyazovskiy et al. 2009; Fig. S17), coupling need not be directly affected by absolute changes in firing rate if neurons fire less but still in temporal alignment. Notably, our SNPC measure was corrected for changes in baseline firing rate. The slow waves typical of NREM sleep show ON and OFF periods with high-intensity firing and synchronization during the ON periods (Vyazovskiy et al. 2009), but lower firing rate when both periods were combined. This coincides with increased within-area coupling during NREM sleep as shown here, as SNPC is dominated by synchronous periods without being affected by prolonged periods of silence. The overall lack of effect of brain states on between-area coupling suggests that, at least for cortical areas, population coupling may to a large extent be governed by hard-wired connectivity and remains relatively stable between conditions of varying neural activity.

Our data reveal a decrease in within-area coupling in hippocampus during NREM sleep, and suggested a trend of decreased hippocampal coupling to neocortical areas, although our analysis could not confirm the latter result based on an additional bootstrapping test. A mechanism proposed for memory consolidation during sleep posits that, during NREM sleep, widespread slow oscillatory activity coupled with hippocampal sharp-wave ripples is necessary to bind elements coded by cortical and hippocampal networks (Buzsáki and Draguhn 2004; Ji and Wilson, 2006; Battaglia et al. 2011). However, we found no evidence of overall coupling increase in average levels of coupling during NREM sleep. During sleep, precise reactivation between hippocampus and cortex during sharp wave ripples would predict stronger levels of coupling (Rothschild et al. 2017; Skelin et al. 2019), but apart from these brief events, predominantly desynchronized activity (LIA) is found in area CA1 during NREM sleep, compatible with the reported decrease in within-area CA1 coupling (Fig. 8A), as well as with the absence of a strong decrease in CA1-neocortical population coupling (Fig. 8B).

Although the loss of cortical integration has been theorized to be an integral part of the loss of consciousness (Massimini et al. 2005; Alkire et al. 2008), the current data on NREM sleep suggest that on the cell-to-population level, such a loss of integration is not clearly shown. Olcese et al. (2016) showed different results using a nonlinear, information-theoretical measure of functional connectivity, highlighting that different levels of processing at ascending scales of brain function paint varying pictures of brain state effects on functional connectivity. Further elucidation at the level of single neurons, cellular subtypes, distinct states and sub-states (e.g. up or down states) are needed to further progress on this subject.

Broadcasting cells and the implications for conceptualizing meta-networks

Our findings offer a glimpse on the structure and functioning of meta-networks, which may serve to outline a theoretical framework for interpreting the current findings. Meta-networks have been postulated to exist, based on the notion that higher perceptual and cognitive functions likely depend on the cooperation between multiple brains areas, achieving a higher order of integration than can be achieved by single structures operating in isolation (Pennartz 2015, 2022; cf. Buzsáki 1989; Eichenbaum 2000). The current results may offer some initial insights into several principles by which meta-networks may operate.

First, the observation of positive correlations between internal and external coupling gave rise to the hypothesis that broadcasting or "hub" cells may exist—neurons significantly coupled to more than one area. Such cells were indeed identified in all four areas, and especially neurons with an index of three were more often found than expected by chance. The distribution of broadcasting indices did not vary greatly between areas and did not markedly differ between different cell types (Fig. S12). Widely broadcasting cells might indicate important synchronizing nodes in a small-world-like network (Watts and Strogatz 1998; Bassett and Bullmore 2017). Because broadcasters engage in synchronizing relationships with multi-area populations, they may function to integrate information, and dynamically coordinate activity in single-area networks, thus contributing to the formation of meta-networks (Pennartz 2015) or network-of-networks (e.g. Havlin et al. 2015). Notably, broadcasting cells did not show strong within-area coupling, indicating that involvement in the local circuit does not correlate with a cell's broadcasting properties. If, however, broadcasting cells are sufficiently connected to neurons with strong within-area coupling, then such internal coupling can still influence spiking synchronization in multiple connected areas.

Second, even within the four-area configuration we examined, the heterogeneity in SNPC relationships was remarkably high, as illustrated by the lack of a common positive correlation between within- and between-area SNPC amongst pairwise area-to-area comparisons. As yet, the extraction of "common rules" for dynamic SNPC coupling thus remains elusive. Instead, our findings suggest that heterogeneity may reflect a fundamental characteristic of meta-networks in the brain, arising in association with unique functions exerted by individual brain areas within the larger network. This heterogeneity is revealed, for instance, by the diversity of within-area coupling changes associated with transitions between brain states (Fig. 8).

Finally, it is appropriate to re-examine what the functional significance of SNPC may be as regards information coding and transmission in multi-area networks. As SNPC correlated negatively with specific information-coding—illustrated here especially by the spatial selectivity of CA1 cells—this result is most parsimoniously interpreted as an expression of intrinsic network dynamics, offering a time-averaged window on cell-to-population synchronization. Our findings show that single neurons not only synchronize with their local network, but also with other populations in the hippocampal-neocortical network, and may thus primarily function in dynamically organizing communication in such large, cross-areal systems. However, when one adopts the reverse perspective and focuses on those cells that do *not* conform to the population firing regime ("soloists"; Okun et al. 2015), one does identify subgroups of neurons having specific information-processing functions. Desynchronized from internal and/or external networks as these cells are, they may guarantee a required level of sparse neural coding (Goltstein et al. 2015) and prevent the overall network from reaching a state of hyperstability during wakefulness. Thus, our findings support the adagium "less coupling means more coding" (or, in a more popularized and speculative rhyme, "less syncing means more thinking"). In a similar vein, but now in the context of (conscious) perception, they also plea against the idea that more "integration" (as indicated by stronger coupling, given sufficient heterogeneity or differentiation) would imply more experienced content (cf. Tononi et al. 2016), but instead favor the notion of sparsely synchronized, distributed ensembles as coding perceptual experience (Jadhav et al. 2009; Harris et al. 2011; Goltstein et al. 2015; Pennartz 2015, 2022). Therefore, non-coupled cell groups form an intriguing

target of future investigations of ensemble behavior during wakeful, conscious processing, characterized by a desynchronization of the EEG (Destexhe et al. 1999).

Acknowledgments

CRediT authors statement

Reinder Dorman (Conceptualization, Formal analysis, Investigation, Methodology, Software, Validation, Visualization, Writing—original draft, Writing—review and editing), Jeroen Bos (Data curation, Investigation, Methodology, Resources, Software), Martin Vinck (Data curation, Investigation, Methodology, Resources, Software), Pietro Marchesi (Formal analysis, Methodology, Resources, Software, Visualization, Writing—review and editing), Julien Fiorilli (Data curation, Formal analysis, Software, Visualization), Jeannette Lorteije (Project administration, Supervision), Ingrid Reiten (Data curation, Formal analysis, Software, Visualization), Jan Bjaalie (Data curation, Resources, Software, Visualization), Michael Okun (Conceptualization, Resources, Software, Writing—original draft, Writing—review and editing), Cyriel Pennartz (Conceptualization, Formal analysis, Funding acquisition, Methodology, Project administration, Resources, Supervision, Visualization, Writing—original draft, Writing—review and editing).

Supplementary material

Supplementary material is available at *Cerebral Cortex* online.

Funding

Conflict of interest statement: The authors declare no conflict of interest.

Data availability

All relevant data are available from the authors.

References

Adoff MD, Climer JR, Davoudi H, Dombeck DA, Marvin JS, Looger LL. The functional organization of excitatory synaptic input to place cells. *Nat Commun*. 2021:12(3558):1–15.

Agster KL, Burwell RD. Cortical efferents of the perirhinal, postrhinal, and entorhinal cortices of the rat. *Hippocampus*. 2009:19(12): 1159–1186.

Alkire MT, Hudetz AG, Tononi G. Consciousness and anesthesia. *Science*. 2008:322(5903):876–880.

Apergis-Schoute J, Pinto A, Paré D. Muscarinic control of long-range GABAergic inhibition within the rhinal cortices. *J Neurosci*. 2007:27(15):4061–4071.

Arszovszki A, Borhegyi Z, Klausberger T. Three axonal projection routes of individual pyramidal cells in the ventral CA1 hippocampus. *Front Neuroanat*. 2014:8:1–11.

Bachatene L, Bharmauria V, Cattan S, Chanauria N, Rouat J, Molotchnikoff S. Electrophysiological and firing properties of neurons: categorizing soloists and choristers in primary visual cortex. *Neurosci Lett*. 2015:604:103–108.

Barthó P, Hirase H, Monconduit L, Zugaro M, Harris KD, Buzsáki G. Characterization of neocortical principal cells and interneurons by network interactions and extracellular features. *J Neurophysiol*. 2004:92(1):600–608.

Bassett DS, Bullmore ET. Small-world brain networks revisited. *Neuroscientist*. 2017:23(5):499–516.

Battaglia FP, Benchenane K, Sirota A, Pennartz CM, Wiener SI. The hippocampus: hub of brain network communication for memory. *Trends Cogn Sci*. 2011:15(7):310–318.

Bjerke IE, Øvsthus M, Papp EA, Yates SC, Silvestri L, Fiorilli J, Pennartz CMA, Pavone FS, Puchades MA, Leergaard TB, et al. Data integration through brain atlasing: human brain project tools and strategies. *European Psychiatry*. 2018:50: 70–76.

Bos JJ, Vinck M, Van Mourik-Donga LA, Jackson JC, Witter MP, Pennartz CMA. Perirhinal firing patterns are sustained across large spatial segments of the task environment. *Nat Commun*. 2017:8(7491):1–12.

Burwell RD, Amaral DG. Cortical afferents of the perirhinal, postrhinal, and entorhinal cortices of the rat. *J Comp Neurol*. 1998:398: 179–205.

Buzsáki G. Two-stage model of memory trace formation: a role for "noisy" brain states. *Neuroscience*. 1989:31(3):551–570.

Buzsáki G. Theta oscillations in the hippocampus. *Neuron*. 2002:33: 1–16.

Buzsáki G. Hippocampus: network physiology. In: Shepherd GM, Grillner S, editors. *Handbook of brain microcircuits*. 1st ed. New York: Oxford University Press; 2010. pp. 165–174.

Buzsáki G, Draguhn A. Neuronal oscillations in cortical networks. *Science*. 2004:304(5679):1926–1929.

Cardin JA, Carlén M, Meletis K, Knoblich U, Zhang F, Deisseroth K, Tsai LH, Moore CI. Driving fast-spiking cells induces gamma rhythm and controls sensory responses. *Nature*. 2009:459(7247): 663–667.

Clancy KB, Orsolic I, Mrsic-Flogel TD. Locomotion-dependent remapping of distributed cortical networks. *Nat Neurosci*. 2019:22: 778–786.

Csicsvari J, Hirase H, Czurkó A, Mamiya A, Buzsáki G. Oscillatory coupling of hippocampal pyramidal cells and interneurons in the behaving rat. *J Neurosci*. 1999:19(1):274–287.

Csicsvari J, Jamieson B, Wise KD, Buzsáki G. Mechanisms of gamma oscillations in the hippocampus of the behaving rat. *Neuron*. 2003:37(2):311–322.

de Curtis M, Paré D. The rhinal cortices: a wall of inhibition between the neocortex and the hippocampus. *Prog Neurobiol*. 2004:74(2): 101–110.

Deacon TW, Eichenbaum H, Rosenberg P, Eckmann KW. Afferent connections of the perirhinal cortex in the rat. *J Comp Neurol*. 1983:220(2):168–190.

DeCharms RC, Zador A. Neural representation and the cortical code. *Annu Rev Neurosci*. 2000:23:613–647.

Destexhe A, Contreras D, Steriade M. Spatiotemporal analysis of local field potentials and unit discharges in cat cerebral cortex during natural wake and sleep states. *J Neurosci*. 1999:19(11): 4595–4608.

Douglas RJ, Martin KAC. Neuronal circuits of the neocortex. *Annu Rev Neurosci*. 2004:27:419–451.

Douglas RJ, Martin KAC. Canonical cortical circuits. In: Shepherd G, Grillner S, editors. *Handbook of brain microcircuits*. 1st ed. New York: Oxford University Press; 2010. pp. 15–21.

Eichenbaum H. A cortical – hippocampal system. *Nat Rev Neurosci*. 2000:1:41–50.

Ercsey-Ravasz M, Markov NT, Lamy C, VanEssen DC, Knoblauch K, Toroczkai Z, Kennedy H. A predictive network model of cerebral cortical connectivity based on a distance rule. *Neuron*. 2013:80(1): 184–197.

Fiorilli J, Bos JJ, Grande X, Lim J, Düzel E, Pennartz CMA. Reconciling the object and spatial processing views of the perirhinal cortex through task-relevant unitization. *Hippocampus*. 2021:31(7):1–19.

Garner RA, Keller GB. A cortical circuit for audio-visual predictions. *Nat Neurosci*. 2021:25:98–105.

Gentet LJ, Avermann M, Matyas F, Staiger JF, Petersen CCH. Membrane potential dynamics of GABAergic neurons in the barrel cortex of behaving mice. *Neuron*. 2010:65(3):422–435.

Gentet LJ, Kremer Y, Taniguchi H, Huang ZJ, Staiger JF, Petersen CCH. Unique functional properties of somatostatin-expressing GABAergic neurons in mouse barrel cortex. *Nat Neurosci*. 2012:15(4):607–612.

Goltstein PM, Montijn JS, Pennartz CMA. Effects of isoflurane anesthesia on ensemble patterns of Ca2+ activity in mouse V1: reduced direction selectivity independent of increased correlations in cellular activity. *PLoS One*. 2015:10(2):1–31.

Goode TD, Tanaka KZ, Sahay A, McHugh TJ. An integrated index: engrams, place cells, and hippocampal memory. *Neuron*. 2020:107(5):805–820.

Harris KD, Shepherd GMG. *Nat Neurosci*. The neocortical circuit : themes and variations. 2015:18(2):170–181.

Harris KD, Csicsvari J, Hirase H, Dragoi G, Buzsáki G. Organization of cell assemblies in the hippocampus. *Nature*. 2003:424(6948): 552–556.

Harris KD, Bartho P, Chadderton P, Curto C, de la Rocha J, Hollender L, Itskov V, Luczak A, Marguet SL, Renart A, et al. How do neurons work together? Lessons from auditory cortex *Hearing Res*. 2011:271(1–2):37–53.

Harris JA, Mihalas S, Hirokawa KE, Whitesell JD, Choi H, Bernard A, Bohn P, Caldejon S, Casal L, Cho A, et al. Hierarchical organization of cortical and thalamic connectivity. *Nature*. 2019:575(7781): 195–202.

Hartley T, Burgess N, Lever C, Cacucci F, O'Keefe J. Modeling place fields in terms of the cortical inputs to the hippocampus. *Hippocampus*. 2000:10(4):369–379.

Havlin S, Stanley HE, Bashan A, Gao J, Kenett DY. Percolation of interdependent network of networks. *Chaos Solit Fractals*. 2015:72: 4–19.

Iurilli G, Ghezzi D, Olcese U, Lassi G, Nazzaro C, Tonini R, Tucci V, Benfenati F, Medini P. Sound-driven synaptic inhibition in primary visual cortex. *Neuron*. 2012:73(4):814–828.

Jadhav S, Wolfe J, Feldman D. Sparse temporal coding of elementary tactile features during active whisker sensation. *Nat Neurosci*. 2009:12:792–800.

Jeffery JK. Integration of the sensory inputs to place cells: what, where, why, and how? *Hippocampus*. 2007:17(9):775–785.

Ji D, Wilson MA. Coordinated memory replay in the visual cortex and hippocampus during sleep. *Nature Neuroscience*, 2006:10(1): 100–107. https://doi.org/10.1038/nn1825.

Jinno S, Klausberger T, Marton LF, Dalezios Y, Roberts JDB, Fuentealba P, Bushong EA, Henze D, Buzsaki G, Somogyi P. Neuronal diversity in GABAergic long-range projections from the hippocampus. *J Neurosci*. 2007:27(33):8790–8804.

Kealy J, Commins S. The rat perirhinal cortex: a review of anatomy, physiology, plasticity, and function. *Prog Neurobiol*. 2011:93(4): 522–548.

Lansink CS, Bakker M, Buster W, Lankelma J, van der Blom R, Westdorp R, Joosten NJMA, McNaughton BL, Pennartz CMA. A split microdrive for simultaneous multi-electrode recordings from two brain areas in awake small animals. *J Neurosci Meth*. 2007:162: 129–138.

Lansink CS, Goltstein PM, Lankelma JV, McNaughton BL, Long X, Zhang S-J. A spatial map in the somatosensory cortex. 2018. https://doi.org/10.1101/473090.

Lansink CS, Goltstein PM, Lankelma JV, McNaughton BL, Pennartz CMA. Hippocampus Leads Ventral Striatum in Replay of Place-Reward Information. *PLoS Biology*, 2009:7(8):e1000173. https://doi.org/10.1371/journal.pbio.1000173.

Martina M, Royer S, Paré D. Propagation of neocortical inputs in the perirhinal cortex. *J Neurosci*. 2001:21(8):2878–2888.

Massimini M, Ferrarelli F, Huber R, Esser SK, Singh H, Tononi G. Breakdown of cortical effective connectivity during sleep. *Science*. 2005:309(5744):2228–2232.

Mehta MR. From synaptic plasticity to spatial maps and sequence learning. *Hippocampus*. 2015:25(6):756–762.

Meijer GT, Montijn JS, Pennartz CMA, Lansink CS. Audio-visual modulation in mouse V1 depends on cross-modal stimulus configuration and congruency. *J Neurosci*. 2017:37(36):0468–0417.

Meijer GT, Mertens PEC, Pennartz CMA, Olcese U, Lansink CS. The circuit architecture of cortical multisensory processing: distinct functions jointly operating within a common anatomical network. *Prog Neurobiol*. 2019:174:1–15.

Melzer S, Michael M, Caputi A, Eliava M, Fuchs EC, Whittington MA, Monyer H. Long-range-projecting gabaergic neurons modulate inhibition in hippocampus and entorhinal cortex. *Science*. 2012:335(6075):1506–1510.

Mertens PEC, Marchesi P, Ruikes T, Oude LM, Krijger Q, Pennartz CMA, Lansink CS. Coherent mapping of location and head direction across auditory and visual cortex. *Cereb Cortex*. 2023:1–17. https://doi.org/10.1093/cercor/bhad045.

Miller MW, Vogt BA. Direct connections of rat visual cortex with sensory, motor, and association cortices. *Journal of Comparative Neurology*, 1984:226(2):184–202. https://doi.org/10.1002/cne.902260204.

Naber PA, Witter MP, Lopes Da Silva FH. Perirhinal cortex input to the hippocampus in the rat: evidence for parallel pathways, both direct and indirect. A combined physiological and anatomical study. *Eur J Neurosci*. 1999:11(11):4119–4133.

Naber PA, Witter MP, Lopes Da Silva FH. Differential distribution of barrel or visual cortex - evoked responses along the rostro-caudal axis of the peri- and postrhinal cortices. *Brain Res*. 2000:877(2): 298–305.

O'Keefe J, Dostrovsky J. The hippocampus as a spatial map. Preliminary evidence from unit activity in the freely-moving rat. *Brain Res*. 1971:34(1):171–175.

Oh SW, Harris JA, Ng L, Winslow B, Cain N, Mihalas S, Zeng H. A mesoscale connectome of the mouse brain. *Nature*. 2014:508(7495):207–214.

Okun M, Steinmetz NA, Cossell L, Iacaruso MF, Ko H, Barthó P, Moore T, Hofer SB, Mrsic-Flogel TD, Carandini M, et al. Diverse

coupling of neurons to populations in sensory cortex. *Nature*. 2015:521(7553):511–515.

Okun M, Steinmetz NA, Lak A, Dervinis M, Harris KD. Distinct structure of cortical population activity on fast and infraslow timescales. *Cereb Cortex*. 2019:29(5):2196–2210.

Olcese U, Bos JJ, Vinck M, Lankelma JV, van Mourik-Donga LB, Schlumm F, Pennartz CMA. Spike-based functional connectivity in cerebral cortex and hippocampus: loss of global connectivity is coupled to preservation of local connectivity during non-REM sleep. *J Neurosci*. 2016:36(29):7676–7692.

Papp EA, Leergaard TB, Calabrese E, Johnson GA, Bjaalie JG. Waxholm Space atlas of the Sprague Dawley rat brain. *NeuroImage*. 2014:97: 374–386.

Pelletier JG, Apergis J, Paré D. Low-probability transmission of neocortical and entorhinal impulses through the perirhinal cortex. *J Neurophysiol*. 2004:91(5):2079–2089.

Pennartz CMA. *The brain's representational power: on consciousness and the integration of modalities*. Cambridge, MA: MIT Press; 2015.

Pennartz CMA. What is neurorepresentationalism? From neural activity and predictive processing to multi-level representations and conscioussness. *Behav Brain Res*. 2022:432(113969):113969.

Perich MG, Rajan K. Rethinking brain-wide interactions through multi-region 'network of networks' models. *Curr Opin Neurobiol*. 2020:65:146–151.

Puchades MA, Csucs G, Ledergerber D, Leergaard TB, Bjaalie JG. Spatial registration of serial microscopic brain images to three-dimensional reference atlases with the QuickNII tool. *PLoS One*. 2019:14(5):e0216796.

Rothschild G, Eban E, Frank LM. A cortical-hippocampal-cortical loop of information processing during memory consolidation. *Nat Neurosci*. 2017:20(2):251–259.

Sieben K, Roder B, Hanganu-Opatz IL. Oscillatory entrainment of primary somatosensory cortex encodes visual control of tactile processing. *J Neurosci*. 2013:33(13):5736–5749.

Skaggs WE, McNaughtion BI, Gothard KM 1993. An information-theoretic approach to deciphering the hippocampal code. In Hanson SJ, Cowan JD, Giles CL, editors.: *Advances in Neural Information Processing Systems 5*. San Mateo, CA: Morgan Kaufmann Publishers. (pp. 1030–1037).

Skelin I, Kilianski S, McNaughton BL. Hippocampal coupling with cortical and subcortical structures in the context of memory consolidation. *Neurobiol Learn Mem*. 2019:160:21–31.

Somogyi P. Hippocampus: Intrinsic organization. In: Shepherd GM, Grillner S, editors. *Handbook of brain microcircuits*. 1st ed. New York: Oxford University Press; 2010. pp. 148–164.

Squire LR, Zola-Morgan S. The medial temporal lobe memory system. *Science*. 1991:253(5026):1380–1386.

Squire LR, Shimamura AP, Amaral DG. *Memory and the hippocampus: neural models of plasticity*. Elsevier; 1989 pp. 208–239.

Stevens CF, Zador AM. Input synchrony and the irregular firing of cortical neurons. *Nat Neurosci*. 1998:1(3):210–217.

Tononi G, Boly M, Massimini M, Koch C. Integrated information theory: from consciousness to its physical substrate. *Nat Rev Neurosci*. 2016:17(7):450–461.

Van Strien N, Cappaert N, Witter M. The anatomy of memory: an interactive overview of the parahippocampal–hippocampal network. *Nat Rev Neurosci*. 2009:10:272–282.

Vinck M, Bos JJ, Van Mourik-Donga LA, Oplaat KT, Klein GA, Jackson JC, Gentet LJ, Pennartz CMA. Cell-Type and State-Dependent Synchronization among Rodent Somatosensory, Visual, Perirhinal Cortex, and Hippocampus CA1. *Frontiers in Systems Neuroscience*, 2016:9. https://doi.org/10.3389/fnsys.2015.00187undefined.

Vyazovskiy VV, Olcese U, Lazimy YM, Faraguna U, Esser SK, Williams JC, Cirelli C, Tononi G. Cortical firing and sleep homeostasis. *Neuron*. 2009:63–878.

Wang X-J, Kennedy H. Brain structure and dynamics across scales: in search of rules. *Curr Opin Neurobiol*. 2016:37:92–98. https://doi.org/10.1016/j.conb.2015.12.010.

Watts DJ, Strogatz SH. Collective dynamics of 'small-world' networks. *Nature*. 1998:393:440–442.

Whittington JCR, Muller TH, Mark S, Chen G, Barry C, Burgess N, Behrens TEJ. The Tolman-Eichenbaum machine: unifying space and relational memory through generalization in the hippocampal formation. *Cell*. 2020:183(5):1249–1263.e23.

Witter MP, Naber PA, Van Haeften T, Machielsen WCM, Rombouts SARB, Barkhof F, Scheltens P, Lopes Da Silva FH. Cortico-hippocampal communication by way of parallel parahippocampal-subicular pathways. *Hippocampus*. 2000:10(4): 398–410.

Yang S, Yang S, Moreira T, Hoffman G, Carlson GC, Bender KJ, Alger BE, Tang CM. Interlamellar CA1 network in the hippocampus. *Proc Natl Acad Sci USA*. 2014:111(35):12919–12924.

Yuste R. From the neuron doctrine to neural networks. *Nat Rev Neurosci*. 2015:16(8):487–497.

Zakiewicz IM, Bjaalie JG, Leergaard TB. Brain-wide map of efferent projections from rat barrel cortex. *Front Neuroinform*. 2014:8: 1–15.

Zandvakili A, Kohn A. Coordinated neuronal activity enhances corticocortical communication. *Coordinated neural activity [...]*. 2016:87(4):827–839.